objective of this investigation was to evaluate whether percolation is applicable to Σ and, if so, to determine the μ and its dependency on cell type and modulator (C10 or C-CPE). This investigation is expected to further our fundamental knowledge on controlling the drug delivery rate, cell signaling and bio-nanotechnology, including fabrication of devices.

MATERIALS AND METHODS

Antibodies and Materials Mouse anti-claudin-4 as the primary antibody and goat anti-mouse immunoglobulin G (IgG) fluorescein isothiocyanate (FITC) conjugate as the secondary antibody were purchased from Invitrogen (Carlsbad CA, U.S.A.). Dulbecco's modified Eagle's medium (DMEM), phosphate-buffered saline (PBS) and bovine serum albumin (BSA) were from Sigma-Aldrich (St. Louis, MO, U.S.A.). Fetal bovine serum (FBS) was from SAFC Biosciences, U.S.A. Penicillin–streptomycin mixed solution (PSS), non-essential amino acids solution (MEM) and Triton-X were from Nacalai Tesque (Kyoto, Japan). Sodium caprate (C10) and formaldehyde were from Tokyo Chemical Industries (Tokyo, Japan) and Wako Pure Chemical Ind., Ltd. (Osaka, Japan), respectively.

C-CPE Preparation C-CPE consisting of amino acid residues 184–319 of CPE was prepared as previously reported.[7] The C-CPE plasmid was transfected into *Escherichia coli*, resulting in BL21 (DE3) strains for the synthesis of C-CPE. The cells were harvested, resuspended, and then lysed with a sonicator. The lysates were applied to the Ni-column, eluted with imidazole, and then purified using a PD-10 column (GE Healthcare, Japan). The resulting C-CPE solution was stored at −80°C until use.

Cell Culture Madin-Darby canine kidney (MDCK) and human epithelial colorectal adenocarcinoma (Caco-2) cells were cultured on a 24-well Intercell dishes (Kurabo, Osaka, Japan) at 37°C in supplemented DMEM [DMEM/FBS/PSS/MEM=500/50/5/5 in volume] at 95% relative humidity with 5% CO_2. The culture medium was replenished every day until TER to reach a constant value.

TER Assay The resistance was monitored with an ohmmeter, Millicell, (Millipore, Billerica, MA, U.S.A.) every 24 h until the resistance reached a constant value; the resistance of a cell monolayer was calculated by Eq. 1.

$$R_{\mathrm{cell}}(t) = R_{\mathrm{obs}}(t) - R_{\mathrm{med}} \tag{1}$$

Here, $R_{\mathrm{obs}}(t)$, $R_{\mathrm{cell}}(t)$ and R_{med} denote the resistance of the whole system, cell at time t and that of medium, respectively. Note that TER=$A\times R_{\mathrm{cell}}$[15]; A=surface area of a single well. Once the TER reached a constant value, C10 (3 mg/mL) or C-CPE (0.01 mg/mL) was immediately added to the apical or basal compartments, respectively. A typical value of TER for MDCK and Caco-2 was 700 $\Omega\cdot$cm^2 and 250 $\Omega\cdot$cm^2, respectively. $R_{\mathrm{cell}}(t)$ was then monitored every 10 s for 30 min at 37°C; we defined t=0 as the time of treatment with C10 or C-CPE. We adopted Σ (=1/R) rather than TER for analyses hereafter. No deconvolution of the transmission function of the electrodes was made, since the response time was short enough to be ignored; the response time was about 1 s, while the experimental time course was 10^1–10^3 s. At least three independent experiments were performed for each case.

Lactate Dehydrogenase (LDH) Assay In order to evaluate cell damage, we measured LDH activity using the Cytotox 96 Assay kit (Promega, Madison, WI, U.S.A.) following the manufacture's manual. The relative C10 or C-CPE-induced LDH release rate (*LRR*) for each sample was calculated by Eq. (2), where ABS_{S}, ABS_{MAX} and ABS_{MIN} denote the absorbance of samples after 30 min of C10 or C-CPE treatment, treated with 1% Triton-X100 and without C10 or C-CPE treatment, respectively.

$$LRR\,(\%) = \frac{ABS_{\mathrm{S}} - ABS_{\mathrm{MIN}}}{ABS_{\mathrm{MAX}} - ABS_{\mathrm{MIN}}} \times 100 \tag{2}$$

It was found that LRR<5% (C10) and *ca.* 1% (C-CPE) after 30 min of exposure. Cytotoxicity was thus ignorable within the experimental time course.

Immunofluorescence Microscopy (IFM) Cell monolayers cultured on an Intercell dish were fixed with 1% formaldehyde at 4°C for 3 h then incubated with 0.1% Triton X-100 for 15 min. After rinsing with PBS, the fixed cells were blocked with 5% BSA in PBS for 45 min, and then incubated with the primary antibodies for 1 h at room temperature. After rinsing with PBS several times, cells were then incubated with the secondary antibodies for 1 h at room temperature. After rinsing again with PBS, cells were carefully mounted on a glass strip, and images of these cells were taken using a bioimaging microscope (CKX41 and IMT2; Olympus, Tokyo, Japan) equipped with a CCD camera.

THEORETICAL DEVELOPMENT

Equivalent Direct Current (DC) Circuit The equivalent DC circuit is that where the paracellular conductors, consisting of the Σ_{TJ} (TJ) and Σ_{LIS} (lateral intercellular space) in series, connect with Σ_{trans} (transmembrane) and Σ_{other} (other than these three) in parallel.[10] Note that $\Sigma_{\mathrm{TJ}} \ll \Sigma_{\mathrm{LIS}}$ when TJs fully develop.[10] The contribution of Σ_{LIS} could thus be neglected. Consequently, the conductivity at time t is approximately given by Eq. 3.

$$\Sigma_{\mathrm{cell}}(t) \approx \phi_{\mathrm{para}}\Sigma_{\mathrm{TJ}}(t) + \phi_{\mathrm{trans}}\Sigma_{\mathrm{trans}}(t) + \phi_{\mathrm{other}}\Sigma_{\mathrm{other}} \tag{3}$$

Here ϕ_{para}, ϕ_{trans} and ϕ_{other} denote the fraction of paracellular, transcellular and that which is other than the first two, respectively.

Analytical Model and Mathematics As a representation of the TJ, a conductive or a less conductive path is assigned respectively to a conductor of which conductivity is σ_1 or σ_2 ($h=\sigma_2/\sigma_1<1$), therewith defining an RRN, where the fraction of the conductor having σ_1 is p. The barrier property of the less conductive path for various types of cells is reflected in σ_2. Based on the effective medium approximation[16] or renormalization group approach,[17] the expression for the Σ of this RRN is given by Eqs. 4 and 5.[16–18]

$$\Sigma = \sigma_1 |\Delta p|^{\mu} \phi_{\pm}(z) \tag{4}$$

$$z \equiv h/|\Delta p|^{s+\mu} \tag{5}$$

Here, $\Delta p=p-p_{\mathrm{c}}$; p_{c} is the percolation threshold in p. μ and s denote the critical exponent for $\sigma_2=0$ (insulator) and $\sigma_1\rightarrow$infinite (superconductor), respectively. $\phi_{\pm}(z)$ is the scaling function and is given by Eq. 6[18]: the subscript$\pm$denotes the sign of Δp.

$$\phi_+(z) \cong A_{1+} + A_{2+}z + \cdots \quad \text{for } z \ll 1 \text{ and } \Delta p > 0 \quad (6A)$$

$$\phi_-(z) \cong A_{1-}z + A_{2-}z^2 + \cdots \quad \text{for } z \ll 1 \text{ and } \Delta p < 0 \quad (6B)$$

In the case of $z \to 0$, combining Eqs. 4 and 6, we obtain Eq. 7.

$$\Sigma / \sigma_1 \propto \Delta p^{\mu} \quad \text{for } \Delta p > 0 \quad (7A)$$

$$\Sigma / \sigma_1 \propto h^{\mu/(s+\mu)} \to 0 \quad \text{for } \Delta p = 0 \quad (7B)$$

$$\Sigma / \sigma_1 \propto h \times \Delta p^{-s} \to 0 \quad \text{for } \Delta p < 0 \quad (7C)$$

Σ remains approximately constant for $p<p_c$, then starts increasing for $p>p_c$. In the case of $0<z\ll1$, on the other hand, $\square_+(z)$ needs a second term or more in Eq. 6A, deviating from the scaling relationships in 7A. Taking the first two terms in Eq. 6A and comparing with Eq. 7A, one can easily obtain a smaller μ for $0<z\ll1$.

Analysis In general, p is a function of time, $p=f(t)$, so that the Taylor expansion around $t=t_c$ and $p=p_c$ yields Eq. 8, *i.e.*, Δp is proportional to $\Delta t=t-t_c$.

$$\Delta p \approx \left.\frac{\partial f(t)}{\partial t}\right|_{t=t_c} \times \Delta t \quad (8)$$

Combining Eqs. 3, 7 and 8, we obtain Eq. 9 for small $\Delta t>0$ and $z \to 0$ if both $\Sigma_{trans}(t)$ and $\Sigma_{other}(t)$ are constant.

$$\frac{\Sigma_{cell}(t)}{\Sigma_{cell}(t_c)} - 1 \propto \Sigma_{TJ}(t) - \Sigma_{TJ}(t_c) \approx \Sigma_{TJ}(t) \propto \Delta t^{\mu} \quad (9)$$

The kinetics given in Eq. 8 governs the TJ modulation rate through p as described in Eq. 7A, since μ is a universal number depending only on d.

RESULTS

Time Course of Conductance For Caco-2 with C-CPE, $r(t)=\Sigma_{cell}(t)/\Sigma_{cell}(0)$ remains approximately constant (*ca.* 1.1), then starts increasing with an inflection (Fig. 1), recovering well the behavior in Eq. 7 (Fig. 1, inserted graph). This system thus corresponds to $z \to 0$. The $r(t)$ for Caco-2 with C10, on the other hand, increases with t and remains approximately constant, then increases again to show an inflection; such a two-stage behavior in TER (proportional to $1/\Sigma_{cell}$) has been reported before.[12,19,20] Similar behavior is observed for MDCK for both C10 and C-CPE (Fig. 1). Note that the time at such inflection, t_c, is calculated from the inflection point in the $\mathrm{Log}[\Sigma_{cell}(t)/\Sigma_{cell}(0)-1]$ *vs.* $\mathrm{Log}(t)$ plot (Fig. 2). We herein term the early and late stage for $t<t_c$ and $t>t_c$, respectively. In the early stage, $r(t_c)$ increases approximately to 2.0 and 1.6 on average, respectively, for MDCK; Caco-2 by the C10 treatment is comparable to values previously reported (*ca.* 2.0, 1.4).[15,20] The difference in $r(t_c)$ between MDCK and Caco-2 would be due to the difference in the sensitivity to C10.

The value of t_c tends to be larger for an extended incubation after TER to reach a constant, *e.g.*, t_c=360→>900 s for an additional 1-d incubation for MDCK with C10. Such an extended incubation will result in a smaller p at $t=0$ due to more developed TJs, requiring a larger t_c for percolation. If the t_c merely corresponds to a response time, t_c should have been independent of the incubation time.

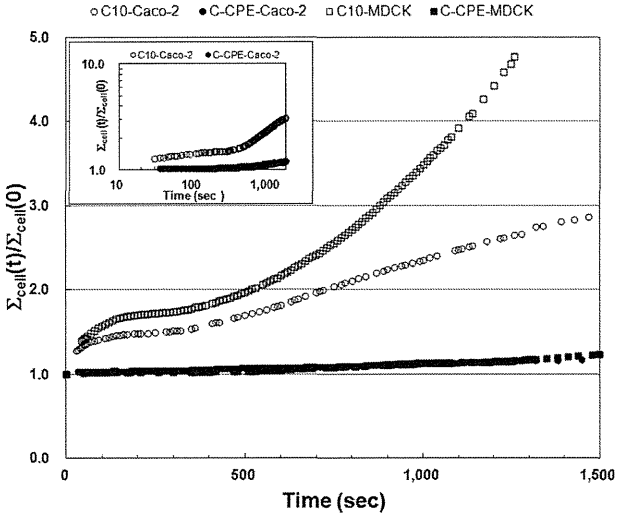

Fig. 1. Time Course of $\Sigma_{cell}(t)/\Sigma_{cell}(0)$ in MDCK and Caco-2

$\Sigma_{cell}(t)/\Sigma_{cell}(0)$ is plotted as a function of t for MDCK and Caco-2 cells. (○): C10-Caco-2; (●): C-CPE-Caco-2; (□): C10-MDCK; and (■): C-CPE-MDCK. Note: a log–log graph for Caco-2 is illustrated in the inserted graph.

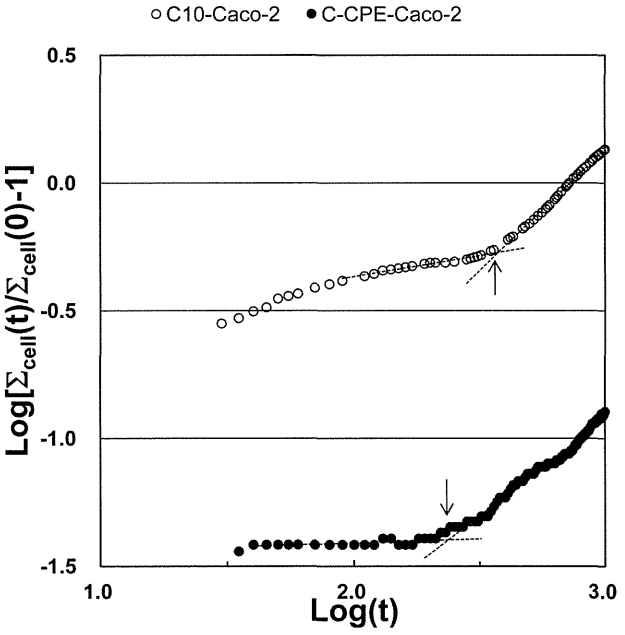

Fig. 2. Relationship between $\mathrm{Log}[\Sigma_{cell}(t)/\Sigma_{cell}(0)-1]$ and $\mathrm{Log}(t)$

$\mathrm{Log}[\Sigma_{cell}(t)/\Sigma_{cell}(0)-1]$ is plotted as a function of $\mathrm{Log}(t)$ to calculate t_c (arrows). The dotted lines are calculated from the least squares regression analysis. (○): representative C10-Caco-2; (●): representative C-CPE-Caco-2.

The plot $\mathrm{Log}[\Sigma_{cell}(t)/\Sigma_{cell}(t_c)-1]$ *vs.* $\mathrm{Log}(\Delta)$ for $\Delta t \geq 0$ (see Eq. 9) yields a straight line (Fig. 3), confirming that the percolation model Eq. 7 is applicable; the slope gives μ.

The Critical Exponent, μ Table 1 summarizes the μ values obtained in this study in addition to those reported based on theoretical and computer simulation for d=2, 3 and for the Bethe lattice.[13,18] We obtain μ=1.1–1.2 regardless the cell type or modulator used, which is close to that for d=2.

Claudin-4 Distribution At $t=0$, claudin-4 localizes at the plasma membrane for both MDCK (Fig. 4, lane 1) and Caco-2 (Fig. 4, lane 2). It should be noted that the localization of claudin-4 at the plasma membrane is not altered even by the additional 24 h of incubation without the treatment by C10 or

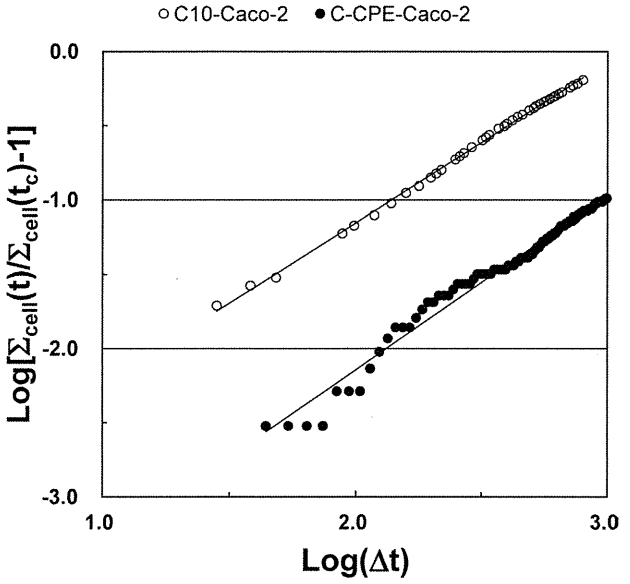

Fig. 3. Relationship between $\mathrm{Log}[\Sigma_{cell}(t)/\Sigma_{cell}(t_c)-1]$ and $\mathrm{Log}(\Delta t)$

$\mathrm{Log}[\Sigma_{cell}(t)/\Sigma_{cell}(t_c)-1]$ is plotted as a function of $\mathrm{Log}(\Delta t)$. (○): C10-Caco-2; (●): C-CPE-Caco-2. The slope, which corresponds to μ, for C10-Caco-2 and C-CPE-Caco-2 is 1.08 (R^2=0.998) and 1.18 (R^2=0.981), respectively. The solid lines are calculated from the least-squares regression analysis.

C-CPE for both cells (Fig. 4, lanes 1, 2 bottom). In both cases, claudin-4 still remains at t=3 min after treatment with C10, while claudin-4 delocalizes and redistributes in the cytoplasm at t=30 min. The PDZ1 domain of ZO-1 associates with the YV motif at the C-terminal of claudin-4.[21] The redistribution of ZO-1 observed in Caco-2[20] would thus result in the redistribution of claudin-4 (Fig. 4). Claudin-4 also remains at the plasma membrane at t=3 min after treatment with C-CPE,

Table 1. The Critical Exponent, μ, Obtained in This Study in Addition to Those for d=2 Square, d=3 Cubic and Bethe Lattice

MDCK	C10	1.18±0.06
MDCK	C-CPE	1.12±0.06
Caco-2	C10	1.15±0.03
Caco-2	C-CPE	1.12±0.05
d=2	Simulation	*ca.* 1.3
d=2	Theory	1.26–1.33
d=3	Simulation	2
d=3	Theory	1.8–2.05
Bethe	Simulation	3
Bethe	Theory	3

then becomes fuzzy (partial delocalization) at t=120 min and finally disappears at t=24 h, being equivalent to patterns previously reported for MDCK.[4] At least the difference in the delocalization rate of claudin-4 would result in the difference in the behavior of Σ_{cell}.

DISCUSSION

***μ* and p_c** We obtain μ= 1.1–1.2 in all cases, implying that the TJ modulation is a d=2 phenomenon. Since TJ modulation takes place in the paracellular space between cells, d=2 is not surprising. The size of the TJ strand network in depth (200–500 nm) is much smaller than the cell size or the distance between tricellular points (10–20 μm), so that the contribution from them would be negligible. The Σ of perforated graphite sheets (d=2, size=50×50) starts increasing at p_c=0.6, and the p_c is close to that for site-percolation on a square lattice.[22] It is, however, difficult in the present system to obtain an exact number of p_c due to the randomness in cell shape[23] (see also Fig. 4). The present system corresponds to

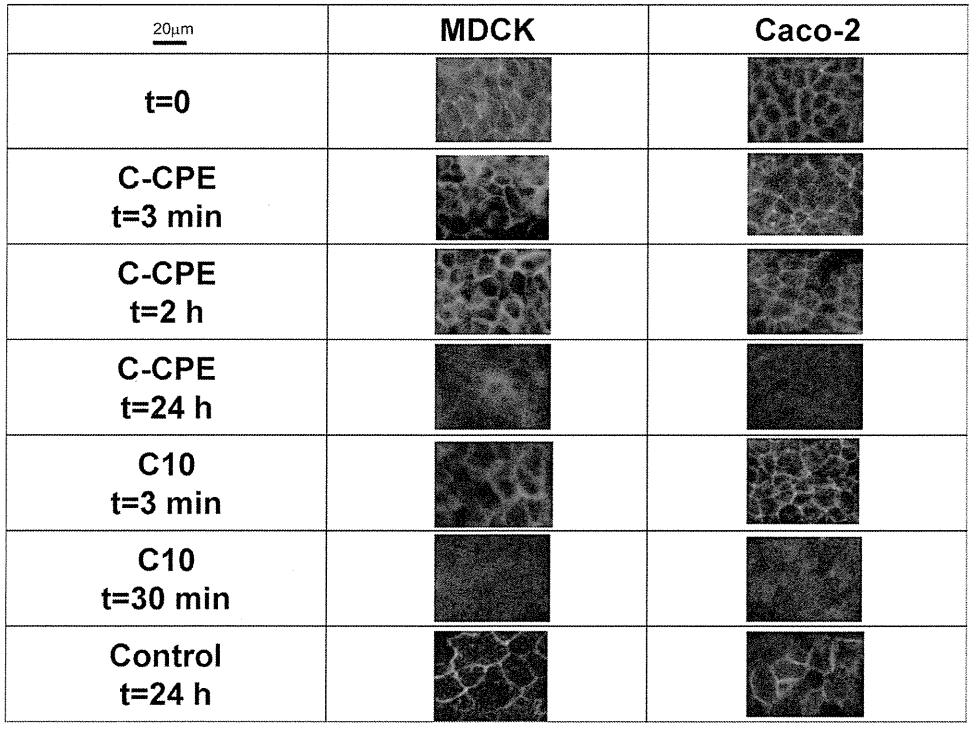

Fig. 4. Time Course of the Distribution of Claudin-4

MDCK (lane-1) and Caco-2 (lane-2).

the bond-percolation and the shape of the cell appears to be between square and hexagonal, so that p_c=0.50–0.65.[13]

Finite Size Effect As previously pointed out, the size of the TJ strand network in the depth direction is much smaller than that in the lateral direction. The system may thus be insufficient as an infinite size. The finite size effect yields smaller values for p_c and μ.[24,25] Indeed, the μ is slightly smaller than that for d=2 (Table 1). At $p=p_c$, finite size scaling for Σ yields Eq. 10, where L_Z and ν denote the system size (proportional to the number of conductors) in depth and the critical exponent for the correlation length, respectively[18,24,25]; ν=4/3 for d=2.

$$\Sigma \propto L_Z^{-\mu/\nu} = L_Z^{-0.975} \approx L_Z^{-1} \quad (10)$$

If L_Z would be proportional to the quantity of claudin-4 (C_{Cldn4}), Σ is approximately inversely proportional to C_{Cldn4}, recovering the results previously pointed out.[26]

Comparison of C10 and C-CPE The following mechanisms will be active upon treatment with C10. Firstly, the expansion of the paracellular gap results in a larger Σ_{TJ} and Σ_{LIS}. This process includes the activation of phospholipase C (PLC), upregulation of intracellular Ca^{2+}, phosphorylation of myosin light chain kinase (MLCK) and actin-myosin filament contraction.[20,27] This is active only in the late stage, since the inhibitor of MLCK is effective only in the late stage[20] despite the rapid elevation (within 1–2 min) of the intracellular Ca^{2+} concentration.[28] Secondly, the delocalization of claudin-4 from the plasma membrane *via* the delocalization of ZO-1[20] or the disruption of lipid rafts[15] increases, at least in Σ_{TJ}. Such delocalization of claudin-4 does not occur within 3 min, but can be seen within 30 min (Fig. 4), consistent with previous reports.[20] Lastly, the membrane perturbation increases in Σ_{trans} within 3 min.[29] This time course is comparable to that seen in the present study. Although the *LRR* is small, and hence leads to a small increase in Σ_{trans}, this contribution may not be ignorable, since the $\square_{trans}$ is large. Furthermore, morphology change may also affect Σ_{other}.

The above first two observations imply that a significant increase in Σ_{TJ} would not be the cause for the increase in $r(t)$ in the early stage. Based on the binary sieving model, not the pore size, but rather the number of pores is altered after C10 treatment,[12] suggesting that p increases, but that σ_1 or σ_2 remains constant. Thus, if Σ_{TJ} mainly controls Σ_{cell} in the early stage, $r(t)$ should have remained approximately constant as observed for C-CPE (Fig. 1); however, this was not the case at all. PLC inhibitors affect both stages.[20] In addition, $r(t)$ increases to 1.2–1.3 at t=200 s, then remains almost constant up to t=1200 s when measured at 4°C, where kinase activity is extremely suppressed. These observations thus suggest that the increase in $r(t)$ in the early stage will be caused at the least by the increase in $\Sigma_{trans}(t)$ *via* membrane perturbation coupled with the elevation of intracellular Ca^{2+}. The early stage is completed by $t=t_c$, since $r(t_c)$ is approximately constant. In contrast, the C-CPE may induce less membrane perturbation, since C-CPE does not penetrate into the plasma membrane.[30] If membrane perturbation occurred, $r(t_c)$ should have been 1.6–2.0 rather than<1.1. The $r(t)$ thus remains approximately constant in the early stage.

Applicability and Limits In the present study, we use MDCK and Caco-2 cell lines, which are epithelial cells from different species and organs. In addition, we use different TJ modulators having different TJ modulation mechanisms. Furthermore, the expression level of claudin isoforms in MDCK and Caco-2 is different especially in claudin-2 and -3.[4,15,31,32] Despite such differences, μ is found to be μ=1.1–1.2 regardless the cell type and TJ modulator. The μ is thus independent of TJ opening mechanisms and claudin isoforms responsible for TJ modulation, suggesting that percolation would be a universal event in Σ. The percolation analysis of this study would thus be applicable to (intestinal) tissue, which is a multilayer system. However, μ for such tissue would be different from that for a cell monolayer. The conductive paths between cell layers may contribute to Σ. In this case, the interaction between layers should be considered. The d may thus be d>2, resulting in a greater value of μ (compare μ for d=2, 3 in Table 1). Generally, d depends on the topology (or connection pattern) of conductive paths.

The diffusion of macromolecular drugs, including proteins and DNA, through TJs has become more important. Due to the analogy between Σ and diffusion coefficient (D),[13] current percolation analysis can be applicable to the diffusion through TJ. The evaluation and control of μ would thus be important in establishing effective drug delivery systems.

The applicability of this percolation analysis is limited under several conditions. Firstly, the scaling form Eq. 7A is not appropriate for leaky TJ, where $h\to1$ (z<1), and the slope, $\partial \mathrm{Log}(\Sigma)/\partial \mathrm{Log}(\Delta p)$, is no longer a constant near $p=p_c$ and becomes smaller, as discussed previously[17,18] (see also Eq. 6). For instance, Σ is a constant, and hence $\mu=\partial \mathrm{Log}(\Sigma)/\partial \mathrm{Log}(\Delta p)=0$, when h=1. In this case, detailed information on $\Sigma_{TJ}(t_c)$ is necessary (see Eq. 9). Secondly, if $\Sigma_{trans}(t)$ or $\Sigma_{other}(t)$ decreases beyond $t>t_c$, Eq. 9 is not a good approximation, yielding a larger number of μ. In this case, the contribution from $\Sigma_{trans}(t)$ and/or $\Sigma_{other}(t)$ should be subtracted. This occurrence may depend on cell type, modulator and their concentration,[12,15,20] although this was not the case in the present study.

CONCLUSION

The time course of electrical conductivity, Σ, in MDCK or Caco-2 cell monolayers upon treatment with C-CPE or C10 was investigated. We found that Σ of TJ could be described within a framework of percolation and determined the critical exponent, μ, to be 1.1–1.2, corresponding to that for d=2 regardless of the cell type or modulator used. TJ modulation is thus a two-dimensional phenomenon, and percolation is the operative mechanism in Σ. Due to the analogy between Σ and D, current percolation analysis can be applicable to the diffusion through TJ and provide important knowledge especially in establishing effective drug delivery systems through the control of μ. However, the applicability of percolation analysis is limited to tight TJ strands ($h\ll1$).

Acknowledgement This work was supported by a Grant-in-Aid for Scientific Research C (21590178) from the Ministry of Education, Culture, Sports, Science and Technology of Japan.

REFERENCES

1) González-Mariscal L, Nava P, Hernández S. Critical role of tight junctions in drug delivery across epithelial and endothelial cell

layers. *J. Membr. Biol.*, **207**, 55–68 (2005).
2) Salama NN, Eddington ND, Fasano A. Tight junction modulation and its relationship to drug delivery. *Adv. Drug Deliv. Rev.*, **58**, 15–28 (2006).
3) Johnson LG. Applications of imaging techniques to studies of epithelial tight junctions. *Adv. Drug Deliv. Rev.*, **57**, 111–121 (2005).
4) Sonoda N, Furuse M, Sasaki H, Yonemura S, Katahira J, Horiguchi Y, Tsukita S. *Clostridium perfringens* enterotoxin fragment removes specific claudins from tight junction strands: Evidence for direct involvement of claudins in tight junction barrier. *J. Cell Biol.*, **147**, 195–204 (1999).
5) Furuse M, Sasaki H, Tsukita S. Manner of interaction of heterogeneous claudin species within and between tight junction strands. *J. Cell Biol.*, **147**, 891–903 (1999).
6) Sasaki H, Matsui C, Furuse K, Mimori-Kiyosue Y, Furuse M, Tsukita S. Dynamic behavior of paired claudin strands within apposing plasma membranes. *Proc. Natl. Acad. Sci. U.S.A.*, **100**, 3971–3976 (2003).
7) Kondoh M, Masuyama A, Takahashi A, Asano N, Mizuguchi H, Koizumi N, Fujii M, Hayakawa T, Horiguchi Y, Watanbe Y. A novel strategy for the enhancement of drug absorption using a claudin modulator. *Mol. Pharmacol.*, **67**, 749–756 (2005).
8) Tomita M, Hayashi M, Awazu S. Absorption-enhancing mechanism of sodium caprate and decanoylcarnitine in Caco-2 cells. *J. Pharmacol. Exp. Ther.*, **272**, 739–743 (1995).
9) Furuse M. Molecular basis of the core structure of tight junctions. *Cold Spring Harb. Perspect. Biol.*, **2**, a002907 (2010).
10) Anderson JM, Van Itallie CM. Physiology and function of the tight junction. *Cold Spring Harb. Perspect. Biol.*, **1**, a002584 (2009).
11) Claude P. Morphological factors influencing transepithelial permeability: a model for the resistance of the zonula occludens. *J. Membr. Biol.*, **39**, 219–232 (1978).
12) Watson CJ, Rowland M, Warhurst G. Functional modeling of tight junctions in intestinal cell monolayers using polyethylene glycol oligomers. *Am. J. Physiol. Cell Physiol.*, **281**, C388–C397 (2001).
13) Stauffer D, Aharony A. *Introduction to Percolation Theory*, 2nd ed., Taylor and Francis, London (1994).
14) Shafrir Y, ben-Avraham D, Forgacs G. Trafficking and signaling through the cytoskeleton: a specific mechanism. *J. Cell Sci.*, **113**, 2747–2757 (2000).
15) Sugibayashi K, Onuki Y, Takayama K. Displacement of tight junction proteins from detergent-resistant membrane domains by treatment with sodium caprate. *Eur. J. Pharm. Sci.*, **36**, 246–253 (2009).
16) Kirkpatrick S. Percolation and conduction. *Rev. Mod. Phys.*, **45**, 574–588 (1973).
17) Costa UMS, Tsallis C, Schwachheim G. Conductivity of a square-lattice bond-mixed resistor network. *Phys. Rev. B Condens. Matter*, **33**, 510–514 (1986).
18) Clerc JP, Giraud G, Laugier JM, Luck JM. The electrical conductivity of binary disordered systems, percolation clusters, fractals and related models. *Adv. Phys.*, **39**, 191–309 (1990).
19) Söderholm JD, Olaison G, Peterson KH, Franzén LE, Lindmark T, Wirén M, Tagesson C, Sjödahl R. Augmented increase in tight junction permeability by luminal stimuli in the non-inflamed ileum of Crohn's disease. *Gut*, **50**, 307–313 (2002).
20) Lindmark T, Kimura Y, Artursson P. Absorption enhancement through intracellular regulation of tight junction permeability by medium chain fatty acids in Caco-2 cells. *J. Pharmacol. Exp. Ther.*, **284**, 362–369 (1998).
21) Itoh M, Furuse M, Morita K, Kubota K, Saitou M, Tsukita S. Direct binding of three tight junction-associated MAGUKs, ZO-1, ZO-2, and ZO-3, with the COOH termini of claudins. *J. Cell Biol.*, **147**, 1351–1363 (1999).
22) Last BJ, Thouless DJ. Percolation theory and electrical conductivity. *Phys. Rev. Lett.*, **27**, 1719–1721 (1971).
23) Hsu HP, Huang MC. Percolation thresholds, critical exponents, and scaling functions on planar random lattices and their duals. *Phys. Rev. E Stat. Phys. Plasmas Fluids Relat. Interdiscip. Topics*, **60** (6 Pt A), 6361–6370 (1999).
24) Sahimi M, Hughes BD, Scriven LE, Davis HT. Critical exponent of percolation conductivity by finite-size scaling. *J. Phys. C Solid State Phys.*, **16**, L521–L527 (1983).
25) Cardy J. *Scaling and Renormalization in Statistical Physics*, Cambridge Lecture Notes in Physics 5, Cambridge University Press, Cambridge (1997).
26) Van Itallie C, Rahner C, Anderson JM. Regulated expression of claudin-4 decreases paracellular conductance through a selective decrease in sodium permeability. *J. Clin. Invest.*, **107**, 1319–1327 (2001).
27) Hayashi M, Sakai T, Hasegawa Y, Nishikawahara T, Tomioka H, Iida A, Shimizu N, Tomita M, Awazu S. Physiological mechanism for enhancement of paracellular drug transport. *J. Control. Release*, **62**, 141–148 (1999).
28) Tomita M, Hayashi M, Awazu S. Absorption-enhancing mechanism of EDTA, caprate, and decanoylcarnitine in Caco-2 cells. *J. Pharm. Sci.*, **85**, 608–611 (1996).
29) Tomita M, Hayashi M, Horie T, Ishizawa T, Awazu S. Enhancement of colonic drug absorption by the transcellular permeation route. *Pharm. Res.*, **5**, 786–789 (1988).
30) Takahashi A, Kondoh M, Masuyama A, Fujii M, Mizuguchi H, Horiguchi Y, Watanabe Y. Role of C-terminal regions of the C-terminal fragment of *Clostridium perfringens* enterotoxin in its interaction with claudin-4. *J. Control. Release*, **108**, 56–62 (2005).
31) McLaughlin J, Padfield PJ, Burt JP, O'Neill CA. Ochratoxin A increases permeability through tight junctions by removal of specific claudin isoforms. *Am. J. Physiol. Cell Physiol.*, **287**, C1412–C1417 (2004).
32) Doi N, Tomita M, Hayashi M. Absorption enhancement effect of acylcarnitines through changes in tight junction protein in Caco-2 cell monolayers. *Drug Metab. Pharmacokinet.*, **26**, 162–170 (2011).

Laboratories of Bio-Functional Molecular Chemistry[1] and Toxicology and Safety Science[2], Graduate School of Pharmaceutical Sciences, Osaka University, Japan

Hepatotoxicity of sub-nanosized platinum particles in mice

Y. YAMAGISHI[1], A. WATARI[1], Y. HAYATA[1], X. LI[1], M. KONDOH[1], Y. TSUTSUMI[2], K. YAGI[1]

Received July 19, 2012, accepted August 30, 2012

Dr. Akihiro Watari, Laboratory of Bio-Functional Molecular Chemistry, Graduate School of Pharmaceutical Sciences, Osaka University, Suita, Osaka 565-0871, Japan
akihiro@phs.osaka-u.ac.jp

Pharmazie 68: 178–182 (2013) *doi: 10.1691/ph.2013.2141*

Nano-sized materials are widely used in consumer products, medical devices and engineered pharmaceuticals. Advances in nanotechnology have resulted in materials smaller than the nanoscale, but the biologic safety of the sub-nanosized materials has not been fully assessed. In this study, we evaluated the toxic effects of sub-nanosized platinum particles (snPt) in the mouse liver. After intravenous administration of snPt (15 mg/kg body weight) into mice, histological analysis revealed acute hepatic injury, and biochemical analysis showed increased levels of serum markers of liver injury and inflammatory cytokines. In contrast, administration of nano-sized platinum particles did not produce these abnormalities. Furthermore, snPt induced cytotoxicity when directly applied to primary hepatocytes. These data suggest that snPt have the potential to induce hepatotoxicity. These findings provide useful information on the further development of sub-nanosized materials.

1. Introduction

Nanotechnology involves manipulation of matter on the scale of the nanometer and has the potential to improve quality of life via functional products. Nanomaterials are commonly defined as objects with dimensions of 1 to 100 nm and are now widely used in electronics, catalysts, clothing, drugs, diagnostic devices, and cosmetics (Baughman et al. 2002; Patra et al. 2010; Service et al. 2007; Ariga et al. 2010). Recent progress in the field has allowed the creation of sub-nanosized materials that have different physicochemical properties, including improved conductivity, durability and strength. Although these materials may be useful for industrial and scientific purposes, the biologic safety of these materials has not been fully evaluated (Nel et al. 2006; Oberdorster et al. 2005).

Nano-sized platinum particles (nPt) are used for industrial applications and in consumer products, such as cosmetics, supplements and food additives (Gehrke et al. 2011; Horie et al. 2011). The biological influence of exposure to nPt has been previously investigated. For example, nPt has anti-oxidative activity (Watanabe et al. 2009; Onizawa et al. 2009; Kajita et al. 2007), and may be useful for the medical treatment of diseases related to oxidative stress and aging. However, some reports suggest that these substances can induce inflammation in mice or impair DNA integrity (Pelka et al. 2009; Park et al. 2010). Thus, the understanding of the biological influences of nPt has still not been definitively established, and our knowledge regarding the biological effects of sub-nanosized platinum particles (snPt) is severely lacking.

Nano-sized particles can enter and penetrate the lungs, intestines and skin. The degree of penetration depends on the size and surface features of the nano-sized particle. Furthermore, nanoparticles can enter the circulatory system and migrate to various organs, such as the brain, spleen, liver, kidney and muscles (Zhu et al. 2008; Furuyama et al. 2009; Oberdorster et al. 2004; Ai et al. 2011). The liver is a vital organ that is involved in the uptake of nutrients and the elimination of waste products and pathogens from the blood; it is also an important organ for the clearance of nanoparticles. However, some nanoparticles are hepatotoxic (Nishimori et al. 2009a, b; Ji et al. 2009; Cho et al. 2009; Folkmann et al. 2009). In the present study, we investigated the influence of sub-nanosized platinum particles (snPt) on the liver.

2. Investigations and results

To investigate the acute liver toxicity of snPt, we administered snPt (15 mg/kg body weight) into mice by intravenous injection. Histological analysis revealed acute hepatic injury, including vacuole degeneration (Fig. 1). Furthermore, administration of snPt at doses over 15 mg/kg resulted in significant elevation of serum alanine aminotransferase (ALT) and aspartate aminotransferase (AST) levels (Fig. 2A and B) and of interleukin-6 (IL-6) levels (Fig. 2C). ALT and AST levels were increased at 3 h to 24 h after intravenous administration at 20 mg/kg snPt (Fig. 3A and B). Cell viability assessment by WST assay demonstrated that direct treatment of isolated hepatocytes with snPt at concentrations of 0.1, 1, 10, 50 and 100 μg/ml resulted in a dose-dependent decrease in hepatocyte viability when compared with vehicle-treated cells (Fig. 4). These observations suggest that snPt induced inflammation and hepatocyte death.

Previous reports showed that biological influences of nanomaterials vary according to material size (Nishimori et al. 2009a, b; Jiang et al. 2008; Oberdorster et al. 2010). Therefore, we examined whether nPt, with a diameter of approximately 15 nm, leads

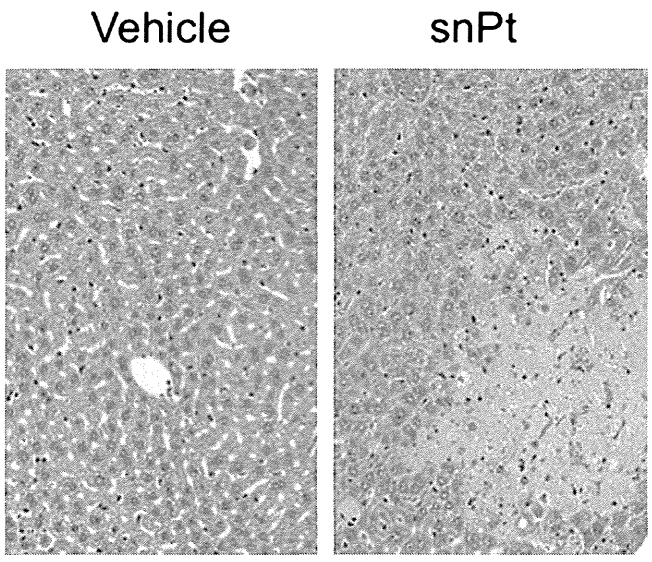

Fig. 1: Histological analysis of liver tissues in snPt-treated mice. snPt was intravenously administered to mice at 15 mg/kg. At 24 h after administration, livers were collected and fixed with 4% paraformaldehyde. Tissue sections were stained with hematoxylin and eosin and observed under a microscope. The pictures show representative data from at least four mice

to a different biologic effect than snPt. As shown in Fig. 5, snPt administration resulted in dose-dependent increases in serum ALT and AST levels, whereas nPt did not. Furthermore, IL-6 levels did not change in response to administration of nPt. These results suggest that the biological effects of platinum particles are dependent on their size.

3. Discussion

The influence of size and of physiochemical properties of nanoparticles on their biologic safety is an important issue. Animal experiments have demonstrated rapid translocation of nanoparticles from the entry site to various organs (Almeida et al. 2011). In particular, nanoparticles tend to concentrate in the liver and are cleared from the body in the feces and urine after intravenous infusion (Ai et al. 2011). While the liver plays a pivotal role in the clearance of nanoparticles, some nanomaterials can induce liver injury. Therefore, we assessed the influence of snPt on the liver and demonstrated that snPt induced liver toxicity *in vitro* and *in vivo*.

Some studies have reported that nPt exert anti-oxidant and anti-inflammatory effects (Watanabe et al. 2009; Onizawa et al. 2009; Kajita et al. 2007), while other studies reported that nPt have negative biological effects. For example, treatment of a human colon carcinoma cell line with nPt resulted in a decrease in cellular glutathione level and impairment in DNA integrity (Pelka et al. 2009). Furthermore, Park et al. (2010) found that nPt prepared from K_2PtCl_6 may induce an inflammatory response in mice. In this study, we found that snPt damaged liver tissues and induced inflammatory cytokines. Kupffer cells present in liver sinusoids may mediate this process via phagocytosis of the particles and subsequent release of inflammatory cytokines. However, when we added snPt to primary hepatocytes, the viability of the cells was significantly reduced, suggesting that snPt may also exert a direct hepatotoxic effect. Thus, the cellular influences of Pt nano- and sub-nano particles may be dependent on the target cells as well as on the size and physical and chemical properties of the particles.

snPt may damage other tissues as well. Cisplatin, a first-line chemotherapy for most cancers, is a platinating agent that can cause kidney damage (Daugaard et al. 1990; Brabec et al. 2005). Furthermore, snPt-induced increases in systemic IL-6 may cause damage to various organs. Further analysis of the distribution and toxic effects of snPt is necessary.

Widespread application of sub-nanosized materials comes with an increased risk of human exposure and environmental release, and the future of nanotechnology will depend on the public acceptance of the risk-benefit ratio. The present study demonstrated that snPt induces hepatotoxicity *in vitro* and *in vivo*. However, our research also indicates that the toxicity of platinum particles could be reduced by altering their size. Additionally, biocompatible coatings can reduce the negative effects of nanoparticles on cells (Oberdorster et al. 2010; Nabeshi et al. 2011; Singh et al. 2007; Clift et al. 2008). Therefore, future studies will contribute to the development of sub-nanosized materials and will also help produce safer products.

4. Experimental

4.1. Materials

Platinum particles with a diameter of 15 nm (nPt) and less than 1 nm (snPt) were purchased from Polytech & Net GmbH (Rostock, Germany). The

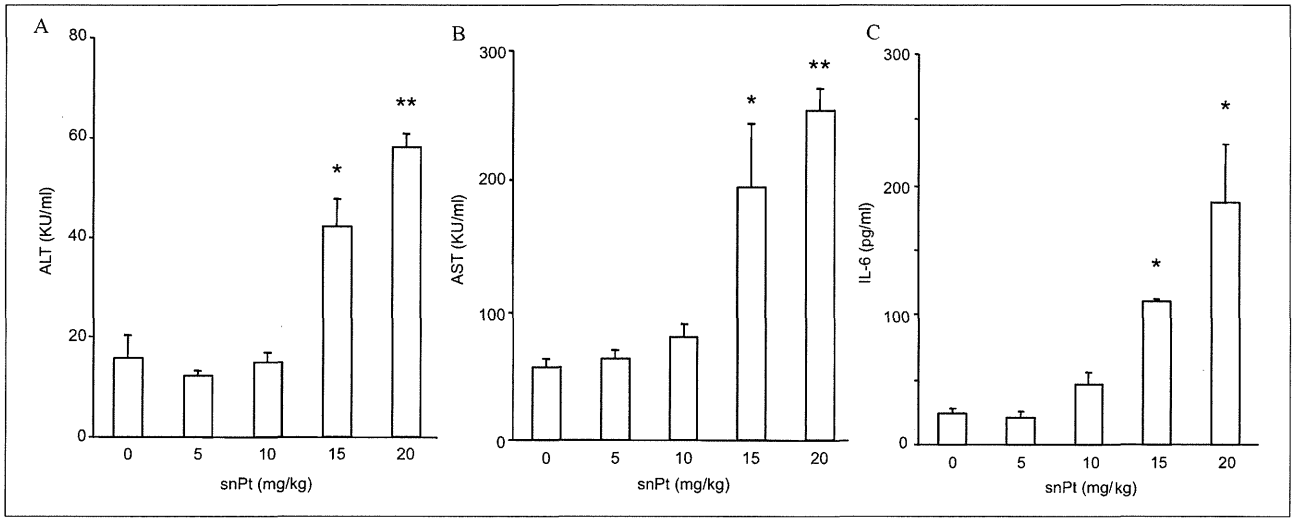

Fig. 2: Dose dependency of snPt-induced liver injury. snPt was intravenously administrated at 5, 10, 15 and 20 mg/kg. At 24 h after administration, blood was recovered, and the resultant serum was used for measurement of ALT (A), AST (B) and IL-6 (C), as described in the "Experimental" section. Data are means ± SEM (n = 3). *Significant difference when compared with the vehicle-treated group (*, $p < 0.05$, **, $p < 0.01$)

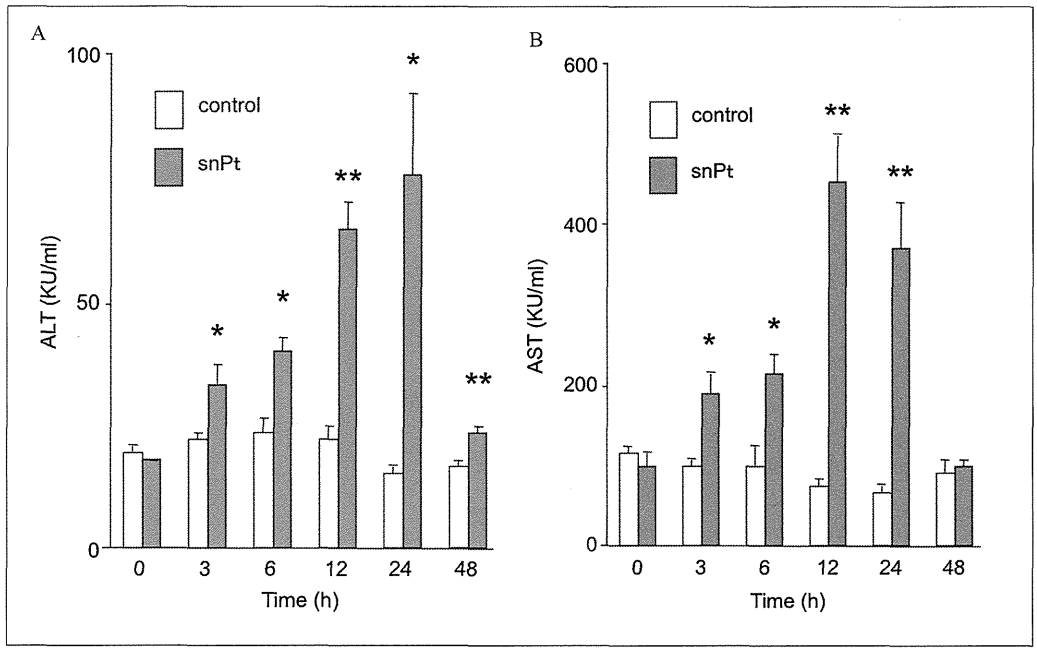

Fig. 3: Time-dependent changes of a biological marker of liver injury. snPt was intravenously administered to mice at 15 mg/kg. Blood was recovered at 3, 6, 12, 24 and 48 h after administration. The serum was used for measurement of ALT (A) and AST (B), as described in the "Experimental" section. Data are means ± SEM (n = 3). *Significant difference when compared with the vehicle-treated group (*, $p < 0.05$, **, $p < 0.01$)

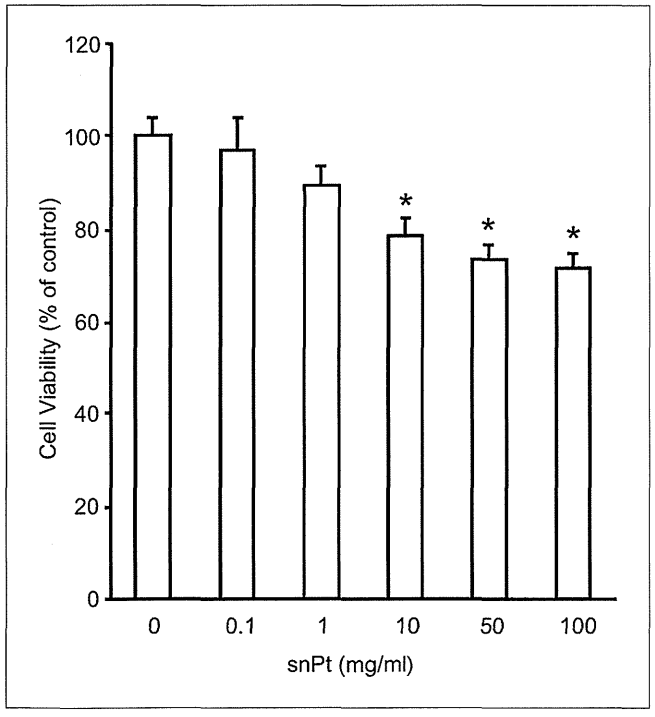

Fig. 4: Cytotoxicity of snPt in hepatic cells. Primary hepatocytes were treated with snPt at 0.1, 1, 10, 50 or 100 μg/ml. After 24 h of culture, cell viability was evaluated with the WST assay, as described in the "Experimental" section. Data are means ± SEM (n = 3). *Significant difference when compared with the vehicle-treated group ($P < 0.05$)

particles were stocked in a 5 mg/ml aqueous suspension. The stock solutions were suspended using a vortex mixer before use. Reagents used in this study were of research grade.

4.2. Animals

BALB/c male mice (8 weeks old) were obtained from Shimizu Laboratory Supplies Co., Ltd. (Kyoto, Japan), and were housed in an environmentally controlled room at 23 ± 1.5 °C with a 12 h light/12 h dark cycle. Mice had access to water and commercial chow (Type MF, Oriental Yeast, Tokyo, Japan). Mice were intravenously injected with nPt or snPt at 5 to 20 mg/kg body weight. The experimental protocols conformed to the ethical guidelines of the Graduate School of Pharmaceutical Sciences, Osaka University.

4.3. Cells

Mouse primary hepatocytes were isolated from BALB/c mice (Shimizu Laboratory Supplies Co.) by the collagenase-perfusion method (Seglen 1976). Isolated hepatocytes were suspended in Williams' E medium containing 10% fetal calf serum, 1 nM insulin, and 1 nM dexamethasone. Next, cell viability was assessed by Trypan blue dye exclusion. Cells that were at least 90% viable were used in this study. Cells were cultured in a humidified 5% CO_2 incubator at 37 °C.

4.4. Histological analysis

After intravenous administration of snPt, mouse livers were removed and fixed with 4% paraformaldehyde. Thin tissue sections were stained with hematoxylin and eosin for histological observation.

4.5. Biochemical assay

Serum alanine aminotransferase (ALT) and aspartate aminotransferase (AST) were measured using commercially available kits (WAKO Pure Chemical, Osaka, Japan), respectively. Interleukin-6 (IL-6) levels were measured with an ELISA kit (BioSource International, Camarillo, CA, USA). These assays were performed according to the manufacturer's protocols.

4.6. Cell viability assay

Cell viability was determined using WST-8 (Nacalai Tesque, Osaka, Japan), according to the manufacturer's protocol. Briefly, 1×10^4 cells/well were seeded on a 96 well plate at 37 °C overnight. After 24 h of treatment with snPt, WST-8 reagent was added to each well. The plate was incubated for 1 h at 37 °C and assessed at an absorbance of 450 nm by a plate reader. Obtained data were normalized to the control group, which was designated as 100%.

4.7. Statistical analysis

Data are presented as means ± SD. Statistical analysis was performed by student's t-test. $P < 0.05$ was considered statistically significant.

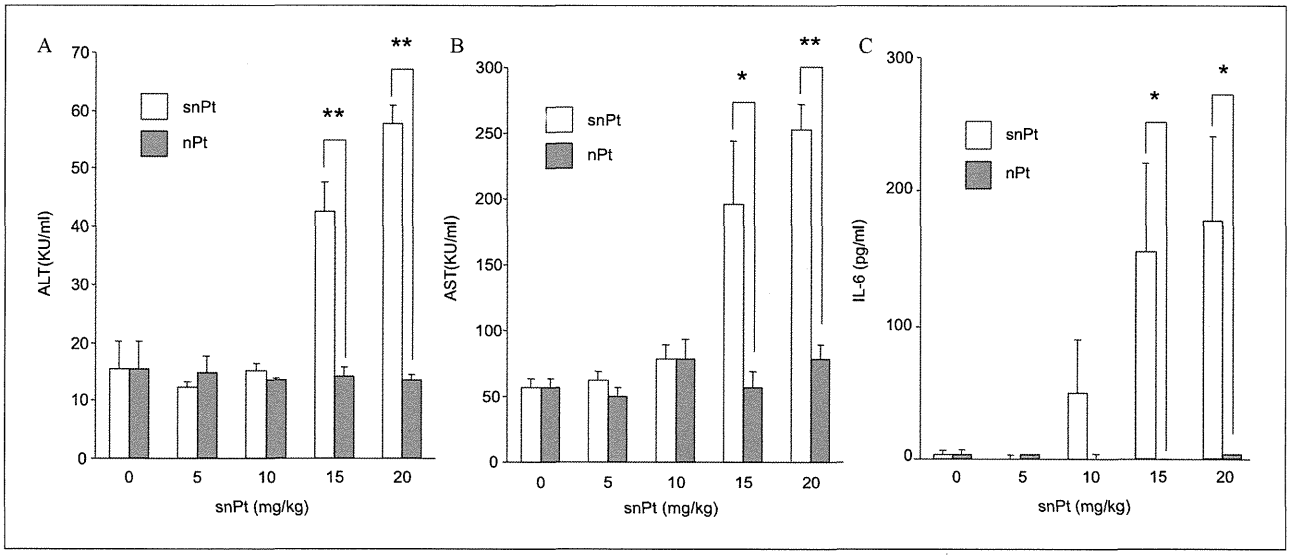

Fig. 5: Effect of particle size of platinum on liver injury. snPt or nPt was intravenously injected into mice at the indicated doses. Blood was recovered at 24 h after injection. Serum ALT (A), AST (B) and IL-6 (C) levels were measured. Data are means ± SEM (n = 3). *Significant difference between the snPt- and nPt-treated groups (*, $p < 0.05$, **, $p < 0.01$)

Acknowledgements: The authors thank all members of our laboratory for useful comments. This study was partly supported by a grant from the Ministry of Health, Labour, and Welfare of Japan.

References

Ai J, Biazar E, Jafarpour M, Montazeri M, Majdi A, Aminifard S, Zafari M, Akbari HR, Rad HG (2011) Nanotoxicology and nanoparticle safety in biomedical designs. Int J Nanomed 6: 1117–1127.

Almeida JP, Chen AL, Foster A, Drezek R (2011) *In vivo* biodistribution of nanoparticles. Nanomedicine (Lond) 6: 815–835.

Ariga K, Hu X, Mandal S, Hill JP (2010) By what means should nanoscaled materials be constructed: molecule, medium, or human? Nanoscale 2: 198–214.

Baughman RH, Zakhidov AA, de Heer WA (2002) Carbon nanotubes–the route toward applications. Science 297: 787–792.

Brabec V, Kasparkova J (2005) Modifications of DNA by platinum complexes. Relation to resistance of tumors to platinum antitumor drugs. Drug Resist Updat 8: 131–146.

Cho WS, Cho M, Jeong J, Choi M, Cho HY, Han BS, Kim HO, Lim YT, Chung BH, Jeong J (2009) Acute toxicity and pharmacokinetics of 13 nm-sized PEG-coated gold nanoparticles. Toxicol Appl Pharmacol 236: 16–24.

Clift MJ, Rothen-Rutishauser B, Brown DM, Duffin R, Donaldson K, Proudfoot L, Guy K, Stone V (2008) The impact of different nanoparticle surface chemistry and size on uptake and toxicity in a murine macrophage cell line. Toxicol Appl Pharmacol 232: 418–427.

Daugaard G (1990) Cisplatin nephrotoxicity: experimental and clinical studies. Dan Med Bull 37: 1–12.

Folkmann JK, Risom L, Jacobsen NR, Wallin H, Loft S, Moller P (2009) Oxidatively damaged DNA in rats exposed by oral gavage to C60 fullerenes and single-walled carbon nanotubes. Environ Health Perspect 117: 703–708.

Furuyama A, Kanno S, Kobayashi T, Hirano S (2009) Extrapulmonary translocation of intratracheally instilled fine and ultrafine particles via direct and alveolar macrophage-associated routes. Arch Toxicol 83: 429–437.

Gehrke H, Pelka J, Hartinger CG, Blank H, Bleimund F, Schneider R, Gerthsen D, Brase S, Crone M, Turk M, Marko D (2011) Platinum nanoparticles and their cellular uptake and DNA platination at non-cytotoxic concentrations. Arch Toxicol 85: 799–812.

Horie M, Kato H, Endoh S, Fujita K, Nishio K, Komaba LK, Fukui H, Nakamura A, Miyauchi A, Nakazato T, Kinugasa S, Yoshida Y, Hagihara Y, Morimoto Y, Iwahashi H (2011) Evaluation of cellular influences of platinum nanoparticles by stable medium dispersion. Metallomics 3: 1244–1252.

Ji Z, Zhang D, Li L, Shen X, Deng X, Dong L, Wu M, Liu Y (2009) The hepatotoxicity of multi-walled carbon nanotubes in mice. Nanotechnology 20: 445101.

Jiang J, Oberdorster G, Elder A, Gelein R, Mercer P, Biswas P (2008) Does Nanoparticle Activity Depend upon Size and Crystal Phase? Nanotoxicology 2: 33–42.

Kajita M, Hikosaka K, Iitsuka M, Kanayama A, Toshima N, Miyamoto Y (2007) Platinum nanoparticle is a useful scavenger of superoxide anion and hydrogen peroxide. Free Radic Res 41: 615–626.

Nabeshi H, Yoshikawa T, Arimori A, Yoshida T, Tochigi S, Hirai T, Akase T, Nagano K, Abe Y, Kamada H, Tsunoda S, Itoh N, Yoshioka Y, Tsutsumi Y (2011) Effect of surface properties of silica nanoparticles on their cytotoxicity and cellular distribution in murine macrophages. Nanoscale Res Lett 6: 93.

Nel A, Xia T, Madler L, Li N (2006) Toxic potential of materials at the nanolevel. Science 311: 622–627.

Nishimori H, Kondoh M, Isoda K, Tsunoda S, Tsutsumi Y, Yagi K (2009) Histological analysis of 70-nm silica particles-induced chronic toxicity in mice. Eur J Pharm Biopharm 72: 626–629.

Nishimori H, Kondoh M, Isoda K, Tsunoda S, Tsutsumi Y, Yagi K (2009) Silica nanoparticles as hepatotoxicants. Eur J Pharm Biopharm 72: 496–501.

Oberdorster G (2010) Safety assessment for nanotechnology and nanomedicine: concepts of nanotoxicology. J Intern Med 267: 89–105.

Oberdorster G, Oberdorster E, Oberdorster J. Nanotoxicology: an emerging discipline evolving from studies of ultrafine particles (2005) Environ Health Perspect 113: 823–839.

Oberdorster G, Sharp Z, Atudorei V, Elder A, Gelein R, Kreyling W, Cox C (2004) Translocation of inhaled ultrafine particles to the brain. Inhal Toxicol 16: 437–445.

Onizawa S, Aoshiba K, Kajita M, Miyamoto Y, Nagai A (2009) Platinum nanoparticle antioxidants inhibit pulmonary inflammation in mice exposed to cigarette smoke. Pulm Pharmacol Ther 22: 340–349.

Park EJ, Kim H, Kim Y, Park K (2010) Intratracheal instillation of platinum nanoparticles may induce inflammatory responses in mice. Arch Pharm Res 33: 727–735.

Patra CR, Bhattacharya R, Mukhopadhyay D, Mukherjee P (2010) Fabrication of gold nanoparticles for targeted therapy in pancreatic cancer. Adv Drug Deliv Rev 62: 346–361.

Pelka J, Gehrke H, Esselen M, Turk M, Crone M, Brase S, Muller T, Blank H, Send W, Zibat V, Brenner P, Schneider R, Gerthsen D, Marko D (2009) Cellular uptake of platinum nanoparticles in human colon carcinoma cells and their impact on cellular redox systems and DNA integrity. Chem Res Toxicol 22: 649–659.

Seglen PO (1976) Preparation of isolated rat liver cells. Methods Cell Biol 13: 29–83.

Service RF. U.S. nanotechnology (2007) Health and safety research slated for sizable gains. Science 315: 926.

Singh S, Shi T, Duffin R, Albrecht C, van Berlo D, Hohr D, Fubini B, Martra G, Fenoglio I, Borm PJ, Schins RP (2007) Endocytosis, oxidative stress and IL-8 expression in human lung epithelial cells upon treatment with fine and ultrafine TiO2: role of the specific surface area and of surface methylation of the particles. Toxicol Appl Pharmacol 222: 141–151.

Watanabe A, Kajita M, Kim J, Kanayama A, Takahashi K, Mashino T, Miyamoto Y (2009) *In vitro* free radical scavenging activity of platinum nanoparticles. Nanotechnology 20: 455105.

Zhu MT, Feng WY, Wang B, Wang TC, Gu YQ, Wang M, Wang Y, Ouyang H, Zhao YL, Chai ZF (2008) Comparative study of pulmonary responses to nano- and submicron-sized ferric oxide in rats. Toxicology 247: 102–111.

Biochemical and Biophysical Research Communications 426 (2012) 454–460

Contents lists available at SciVerse ScienceDirect

Biochemical and Biophysical Research Communications

journal homepage: www.elsevier.com/locate/ybbrc

A simple reporter assay for screening claudin-4 modulators

Akihiro Watari, Kiyohito Yagi, Masuo Kondoh *

Laboratory of Bio-Functional Molecular Chemistry, Graduate School of Pharmaceutical Sciences, Osaka University, Suita, Osaka 565-0871, Japan

ARTICLE INFO

Article history:
Received 15 August 2012
Available online 27 August 2012

Keywords:
Claudin
Tight junction
Reporter assay
Screening
Chemical modulator

ABSTRACT

Claudin-4, a member of a tetra-transmembrane protein family that comprises 27 members, is a key functional and structural component of the tight junction-seal in mucosal epithelium. Modulation of the claudin-4-barrier for drug absorption is now of research interest. Disruption of the claudin-4-seal occurs during inflammation. Therefore, claudin-4 modulators (repressors and inducers) are promising candidates for drug development. However, claudin-4 modulators have never been fully developed. Here, we attempted to design a screening system for claudin-4 modulators by using a reporter assay. We prepared a plasmid vector coding a claudin-4 promoter-driven luciferase gene and established stable reporter gene-expressing cells. We identified thiabendazole, carotene and curcumin as claudin-4 inducers, and potassium carbonate as a claudin-4 repressor by using the reporter cells. They also increased or decreased, respectively, the integrity of the tight junction-seal in Caco-2 cells. This simple reporter system will be a powerful tool for the development of claudin-4 modulators.

1. Introduction

Tight junctions (TJs), the most apical components of intercellular junctional complexes, function as fences that maintain cellular polarity and provide a barrier to regulate intercellular permeability of epithelia [1,2]. Disruption of cellular polarity and the TJ-seal is frequently observed during carcinogenesis and inflammation [3]. Modulation of TJ-seals for drug absorption is now of research interest [4,5]. A series of studies has revealed that TJs are composed of transmembrane proteins (such as occludin and claudins), junction adhesion proteins, and cytoplasmic scaffolding proteins, including ZO-1, ZO-2, and ZO-3 (see reviews [6–8]). Of these, claudins are thought to be the main structural and functional components of TJs.

Claudins, tetra-transmembrane proteins with a molecular mass of approximately 23 kDa, comprise a multigene family containing over 20 members [8]. The barrier-function and the expression patterns of claudin members differ among tissues [6,8,9]. Claudin-1-, -5-, and -11-deficient mice show dysfunction of the epidermal barrier, blood–brain barrier, and blood–testis barrier, respectively [10–12]. The expression levels and the barrier-functions of claudins are often altered in various cancer cells; they can be down-regulated or up-regulated, depending on the type of cancer [13]. Changes in claudin expression have also been observed in the mucosal epithelium under inflammatory conditions [14]. Claudins are thus potent targets for drug development, such as drug delivery, anti-cancer agents, and anti-inflammatory agents.

Since claudins play a role in TJ-seals, modulation of the claudin-barrier is a potent strategy for drug absorption. The carboxyl-terminus of *Clostridium perfringens* enterotoxin (C-CPE) is a modulator of the claudin-barrier [15]. Treatment of cells with C-CPE causes a decrease in claudin-4 proteins in TJs, followed by an enhancement of the paracellular transport of solutes without causing cytotoxicity [15]. C-CPE also enhances jejunal, nasal, and pulmonary absorption of drugs [16]. Thus, proof-of-concept for claudin-targeted drug absorption has been demonstrated. A decrease in claudin-4 in the intestinal epithelium often occurs in colitis [17]. Down-regulation of claudin-4 is also observed in some cancer cells [18]. Induction of claudin-4 is involved in the chemo-preventive effect of nonsteroidal anti-inflammatory drugs [19]. A modulator of claudin-4 expression would therefore be a potent molecule for claudin-targeted drug absorption and drug development for some inflammatory diseases and cancers. However, an effective system to screen for claudin modulators is lacking.

Here, we developed a simple system to monitor claudin-4 expression using a reporter gene, and we screened chemical claudin-4 modulators.

Abbreviations: TJs, tight junctions; C-CPE, the carboxyl terminus of *Clostridium perfringens* enterotoxin; TGF-β, transforming growth factor-β; EGF, epidermal growth factor; PMA, phorbol 12-myristate 13-acetate; DMSO, dimethyl sulfoxide; PCR, polymerase chain reaction; RT-PCR, reverse transcription-PCR; GAPDH, glyceraldehyde 3-phosphate dehydrogenase; qPCR, quantitative PCR; SDS, sodium dodecyl sulfate; SDS-PAGE, SDS-polyacrylamide gel electrophoresis; TER, transepithelial electric resistance.

* Corresponding author. Fax: +81 6 6879 8199.
E-mail address: masuo@phs.osaka-u.ac.jp (M. Kondoh).

0006-291X/$ - see front matter © 2012 Elsevier Inc. All rights reserved.
http://dx.doi.org/10.1016/j.bbrc.2012.08.083

2. Materials and methods

2.1. Reagents and cells

Recombinant human transforming growth factor-β (TGF-β) and epidermal growth factor (EGF) were purchased from R&D systems (Minneapolis, MN) and Peprotech Inc. (Rocky Hill, NJ), respectively. The recombinant proteins were dissolved in water and stored at −80 °C before use. Phorbol 12-myristate 13-acetate (PMA) were dissolved in dimethyl sulfoxide (DMSO) and stored at −20 °C before use. List of the chemicals used in this study for screening for claudin-4 modulator is shown in Table 1. All reagents were of research grade.

MCF-7, and Caco-2 cells were cultured in Dulbecco's modified minimal essential medium supplemented with 10% fetal bovine serum in 5% CO_2 at 37 °C. MCF-7 cells were obtained from the RIKEN cell bank (Ibaragi, Japan). Caco-2 cells were obtained from the American Type Culture Collection (Manassas, VA). MCF-7 cells stably expressing snail or HRasV12 were prepared by infection with a recombinant retroviral vector coding for snail or HRasV12 gene.

2.2. Preparation of a reporter plasmid

Genomic DNA was extracted from MCF-7 cells by using a genomic DNA isolation kit (Sigma–Aldrich, St. Louis, MO). The claudin-4 promoter region was cloned by polymerase chain reaction (PCR) using genomic DNA as a template and paired primers (forward primer, 5′-GCGCTAGCGGTTGCCCCCTGGCCTTAAC-3′; reverse primer, 5′-CGCTCGAGGTCCACGGGAGTTGAGGACC-3′). The resultant fragments (500 bp) were subcloned into the pGV-B2 vector encoding the luciferase gene (Toyobo, Osaka, Japan). The sequence of the claudin-4 promoter region was confirmed.

2.3. A transient expression of transfection snail or HRasV12 gene

Transfection was performed with FuGENE HD (Roche, Mannheim, Germany) according to the manufacturer's protocol. Briefly, cells were seeded onto 24-well plates. When the cells reached to 80% confluent cell density, 20 μl of medium containing 0.6 μl of FuGENE HD and 200 ng of plasmid carrying snail or HRasV12 gene was added to the wells. After 48 h of transfection, the luciferase activity of the cell lysates was measured as described below.

2.4. Luciferase assay

Luciferase activity was measured using a commercial available luciferase assay system (Toyo Ink, Tokyo, Japan). Cells were lysed with a cell lysis reagent, LCβ (Toyo Ink). The cell lysates were then centrifuged at *18,000g* for 5 min. The luciferase activity in the resulting supernatant was measured using a TriStar LB 941 microplate reader (Berthold, Wildbad, Germany).

2.5. Establishment of a stable reporter cell line

MCF-7 cells were transfected with the reporter plasmid and a plasmid carrying the puromycin resistance gene. Stable transfectants were selected in the presence of puromycin.

2.6. Screening for claudin-4 modulators

The clone 35 cells were seeded onto 96-well plates at a density of 4×10^4 cells/well. On the following day, vehicle or compound was added, and the cells were cultured for an additional 24 h. The luciferase activity in the cells was then measured as described above.

2.7. Cytotoxicity assay

Clone 35 cells or Caco-2 cells were seeded onto a 96-well plate at a density of 4×10^4 or 6×10^4 cells/well, respectively. On the following day, cells were treated with chemicals at the indicated periods. The cell viability was measured by using a WST-8 assay kit (Nacalai, Kyoto, Japan).

2.8. Reverse transcription–PCR (RT–PCR) analysis

RT reaction and PCR amplification were performed with a cDNA synthesis kit (Roche, Mannheim, Germany) and ExTaqTM (Takara, Shiga, Japan), respectively, according to the manufacturer's instructions. Briefly, total RNA was prepared with TRIzol reagent (Invitrogen, Carlsbad, CA). For reverse transcription, 5 μg of total RNA was used. PCR was performed for 23 cycles for claudin-4 (94 °C for 30 s, 55 °C for 15 s, 72 °C for 30 s) and for 20 cycles for GADPH (94 °C for 30 s, 55 °C for 15 s, 72 °C for 60 s). The PCR products were separated by use of agarose gel electrophoresis and stained with ethidium bromide. The sequences of the primers are as follows: forward primer for claudin-4, 5′-CAACATTGTCACCTCGCAGACCATC-3′; reverse primer for claudin-4, 5′-TATCACCATAAGGCCGGCCAACAG-3′; forward primer for glyceraldehyde 3-phosphate dehydrogenase (GAPDH), 5′-TCTTCACCACCATGGAGAAG-3′; reverse primer for GAPDH, 5′-ACCACCTGGTGCTCAGTGTA-3′.

2.9. Quantitative PCR (qPCR) analysis

qPCR was performed with SYBR Premix Ex Taq II (Takara) using an Applied Biosystems StepOne Plus (Applied Biosystems, Foster City, CA). Relative quantification was performed against a standard curve and the values were normalized against the input determined for the housekeeping gene, GAPDH. The primer sequences used for qPCR were as follows: forward primer for claudin-4, 5′-TTGTCACCTCGCAGACCATC-3′ and reverse primer for claudin-4, 5′-CAGCGAGTCGTACACCTTG-3′; forward primer for GAPDH, 5′-GGTGGTCTCCTCTGACTTCAACA-3′ and reverse primer for GAPDH, 5′-GTGGTCGTTGAGGGCAATG-3′.

2.10. Western blot analysis

Cells were lysed with RIPA buffer (0.15 M NaCl, 50 mM Tris–HCl, pH 7.4, 1 mM ethylenediaminetetraacetic acid, 1% Triton X-100, 1% sodium deoxycholate, 0.1% sodium dodecyl sulfate (SDS), 1% protease inhibitor cocktail [Sigma–Aldrich]). The cell lysates were subjected to 15% SDS–polyacrylamide gel electrophoresis (SDS–PAGE), followed by blotting onto polyvinylidene difluoride membrane. The membranes were incubated with anti-claudin-4 mouse monoclonal (Zymed, South San Francisco, CA) and anti-β-actin mouse monoclonal (Sigma–Aldrich) antibodies, respectively, and subsequently treated with horseradish peroxidase-conjugated anti-mouse IgG (Zymed). The reactive bands were detected by using an enhanced chemiluminescence reagent (GE Healthcare, Buckinghamshire, UK).

2.11. Transepithelial electric resistance (TER) assay

Caco-2 cells were seeded into Transwell™ chambers (Corning, NY) at a density of 8×10^4 cells/well. On 7 days after the seeding or when TER values reached a plateau, claudin-4 inducers (thiabendazole, carotene, or curcumin) or claudin-4 repressor (potassium carbonate), respectively, was added. The TER values were then monitored at 0, 24, and 48 h using a Millicell-ERS epithelial

Table 1
Chemicals used in this study as screening sources.

Sample number	Sample name	Concentration[a]	Relative luciferase activity[b]
1	Tartrazine	10 mM	1.29
2	Potassium nitrate	1 mM	0.94
3	Potassium carbonate	10 mM	0.56
4	Sodium chlorous	10 mM	0.95
5	Zinc sulfate	0.1 mM	0.95
6	New coccine	0.01 mM	0.98
7	Amaranth (Bordeaux S)	1 mM	1.34
8	Allura red AC	1 mM	1.49
9	Sunset yellow FCF	1 mM	1.59
10	Potassium hydroxide	1 mM	0.83
11	L-ascorbic acid	1 mM	1.02
12	Sodium nitrite	10 mM	0.91
13	Propionic acid	0.0001%	0.82
14	Sodium carbonate	1 mM	0.91
15	Zinc gluconate	0.01%	1.76
16	Benzoic acid	0.01 mM	1.3
17	Sorbic acid	1 mM	1.51
18	Aspartame	1 mM	1.59
19	Dibutylhydroxytoluene	0.01 mM	1.81
20	Allyl isothiocyanate	0.0001%	1.72
21	Saccharin	1 mM	1.5
22	L-Ascorbyl palmitate	1 mM	1.21
23	Hydroxy biphenyl	0.01 mM	1.87
24	Aluminium potassium sulfate	0.1 mM	0.94
25	L-Lysine	10 mM	1.42
26	Calcium pantothenate	10 mM	1.61
27	Carrageenin	0.01 mM	1.56
28	Tartaric acid	1 mM	1.01
29	Sodium acetate	10 mM	1.02
30	Glycine	10 mM	1.68
31	Sodium alginate	10 mM	1.52
32	Ammonium chloride	10 mM	1.91
33	Magnesium sulfate	10 mM	1.56
34	5-Ribonucleotide	0.001 mM	1.15
35	Calcium chloride	1 mM	1.62
36	Valine	10 mM	1.08
37	Erythrosine	0.01 mM	1.22
38	Annatto	0.01 mM	1.96
39	Maltitol	10 mM	1.44
40	Sodium dehydroacetate	1 mM	1.98
41	Nicotinic acid	1 mM	1.55
42	Isoleucine	1 mM	1.06
43	Mannitol	10 mM	1.29
44	Ascorbic acid (Vitamin C)	10 mM	1.17
45	Phenylalanine	1 mM	0.95
46	Gallic acid	0.1 mM	1.41
47	Erythorbic acid (Sodium isoascorbate)	1 mM	1.03
48	Magnesium chloride	0.1%	1.26
49	Cochineal extract	0.1%	1.02
50	Calcium dihydrogen pyrophosphate	1 mM	1.1
51	Calcium citrate	0.01 mM	0.92
52	Polyvinyl acetate	0.1 mM	1.13
53	Fumaric acid	0.01 mM	1.24
54	Sodium methyl *p*-hydroxybenzoate	1 mM	2.04
55	Tocophenol (Vitamin E)	0.0001%	2.14
56	Rennet	0.01%	0.89
57	Ionone	0.01%	1.15
58	Isoeugenol	0.001%	1.15
59	Allyl isosulfocyanate	0.001%	1.06
60	Propylene glycol	0.1%	0.87
61	Ethyl isovalerate	0.001%	0.89
62	Pectin	0.001%	0.98
63	Cysteine	0.01 mM	0.76
64	Tragacanth gum	0.01%	0.83
65	Thiamin	0.1%	1.15
66	Gum arabic	0.01%	0.91
67	Cellulose	0.001%	0.84
68	Thiabendazole	0.1 mM	3.24
69	Isopropyl citrate	10 mM	1.04
70	γ-oryzanol	0.01%	1.02
71	Calcium carbonate	0.001%	0.857
72	Propylene glycol alginate	0.01%	0.87
73	Chlorophyll	0.1%	1.02
74	Sodium chondroitin sulfate	0.1%	1.04

Table 1 (*continued*)

Sample number	Sample name	Concentration[a]	Relative luciferase activity[b]
75	Biphenyl	0.1 mM	0.99
76	Sodium cytidylic acid	1 mM	0.77
77	Stevia rebaudiana	0.01%	0.96
78	Calcium stearoyl lactylate	0.01%	0.83
79	Ferrous sulfate	0.1 mM	1.37
80	Calcium sulfate	0.1 mM	0.93
81	Benzoyl peroxide	0.1 mM	1.13
82	Dibenzoyl thiamine	1 mM	0.88
83	Carotene	0.1 mM	2.09
84	Guar gum	0.001%	0.84
85	Xanthan gum	0.001%	0.77
86	Curcumin	0.01 mM	2.0

[a] The chemical concentrations were set at the maximum level to show no cytotoxicity.
[b] The relative luciferase activities were calculated as the ratio of that in the chemical-treated cells to that in the vehicle-treated cells. The treatment period was 24 h.

volt-ohmmeter (Millipore Corporation, Billerica, MA). The TER values were normalized to the area of the Caco-2 cell monolayers, and the TER value of a blank chamber was subtracted.

3. Results

3.1. Preparation of a reporter plasmid encoding a claudin-4-promoter-driven luciferase gene

As a first step toward developing a simple screening system for claudin-4 modulators, we cloned the promoter region of claudin-4. We searched for a region that was highly conserved among animals by using a UCSC Genome Bioinformatics program and cloned a 500 bp fragment corresponding to −293 to +194 bp of the claudin-4 gene. This 500 bp fragment contained various transcription factor-binding sites: an E-box (−276 to −271, −262 to −257, −221 to −216, −19 to −14, +10 to +14), a smad-binding element (SBE; −212 to −209, −103 to −100, −38 to −35), and Sp1 (−66 to −57, −53 to −44) [20,21], indicating that this region is a potent candidate for a regulatory region of claudin-4 expression. We constructed a reporter expression vector, in which the 500 bp fragment was inserted upstream of a luciferase gene Suppl. Fig. 1A). To

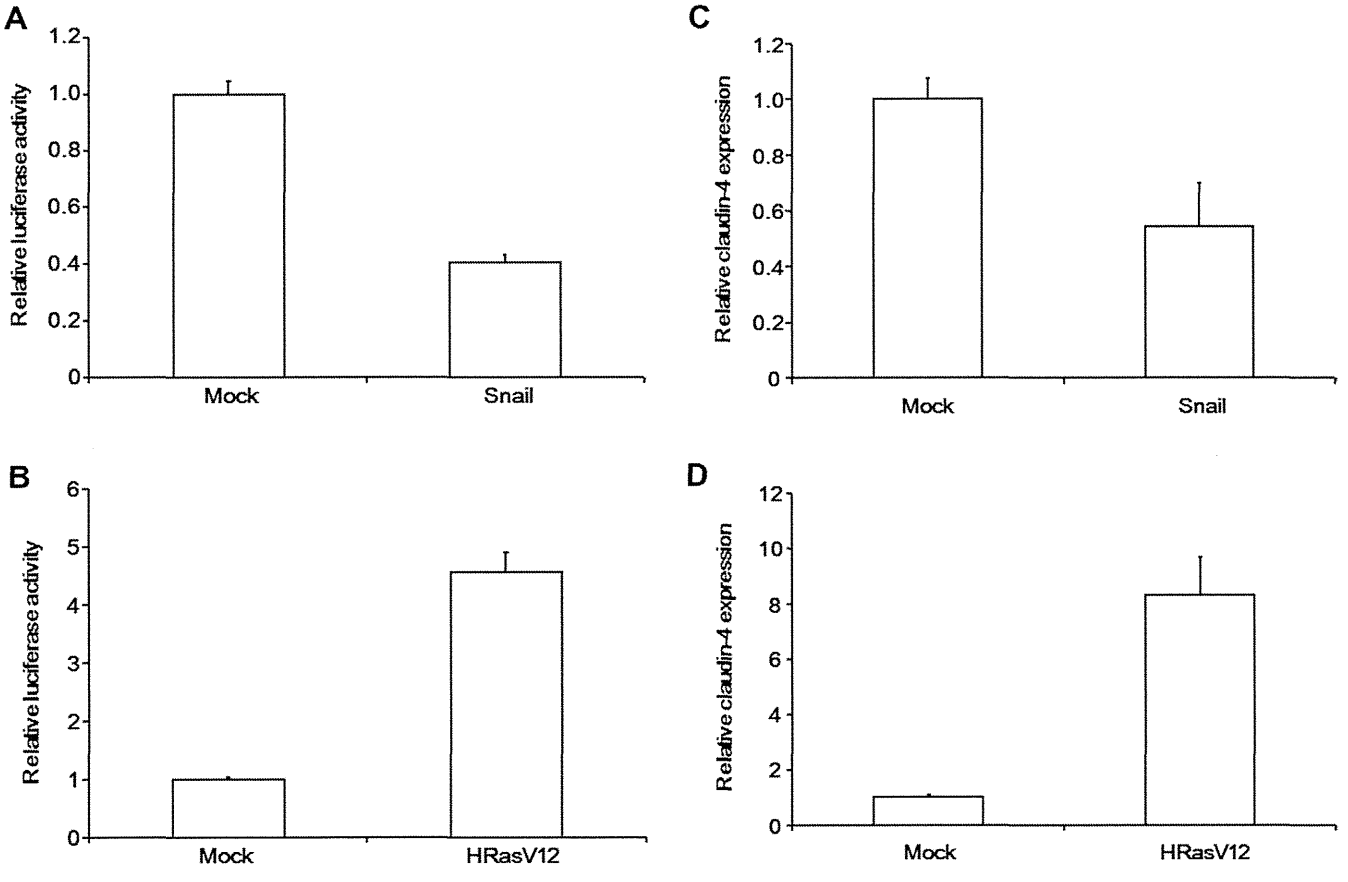

Fig. 1. Preparation of a reporter system monitoring claudin-4 expression. (A, B) Effects of snail and HRasV12 on the luciferase activity in transiently expressing cells. Snail-expressing MCF-7 cells (A) or HRasV12-expressing MCF7 cells (B) were transfected with the claudin-4 reporter plasmid. Two days later, the cells were recovered, and the luciferase activity in the lysates was measured. The data are means ± S.D. ($n = 3$). The results are representative of two independent experiments. (C, D) qPCR analysis of claudin-4 expression in transiently expressing cells. After 2 days of the transfection with the claudin-4 reporter plasmid, total RNA was extracted from snail-expressing MCF-7 cells (C) or HRasV12-expressing MCF-7 cells (D). Expression level of claudin-4 of the transfected cells was quantified by qPCR as described in the Section 2. Claudin-4 expression level was shown as ratio to that of the mock cells. The data are means ± S.D. ($n = 3$). The results are representative of two independent experiments.

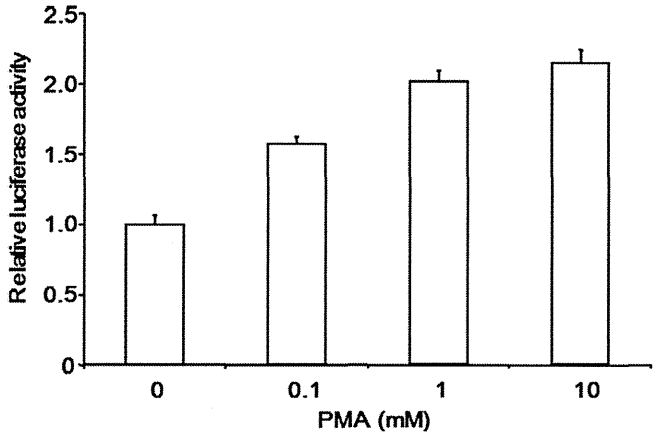

Fig. 2. Effect of PMA on the luciferase activity in clone 35 cells. Clone 35 cells were treated with PMA at the indicated concentrations for 24 h. Luciferase activity in the lysates was measured. The relative luciferase activity is shown as the ratio of the luciferase activity in the treated cells to that of the vehicle-treated cells. The data are means ± S.D. ($n = 3$). The results are representative of two independent experiments.

evaluate expression of the reporter gene, we checked the endogenous claudin-4 expression level in various cell lines and selected MCF-7, HaCat, HT1080, and SiHa cells, which have different claudin-4 expression levels for our analyses (Suppl. Fig. 1B). We transiently transfected the reporter plasmid into these cell lines and found that the luciferase activity of each was correlated with the endogenous expression level of claudin-4 (Suppl. Fig. 1C). We also investigated expression of the reporter gene in MCF-7 cells stably expressing snail or HRasV12, which suppress or induce claudin-4 expression, respectively [22,23]. Transfection of snail- or HRasV12-expressing MCF-7 cells with the reporter plasmid decreased or increased, respectively, the luciferase activity compared to that of mock-transfected MCF-7 cells (Fig. 1A and B). The difference in luciferase activity paralleled the level of claudin-4 mRNA in the cells (Fig. 1C and D), suggesting that the cloned promoter region was functional.

3.2. Preparation of a screening system for claudin-4 modulators

We transfected MCF-7 cells with the claudin-4 reporter plasmid and isolated stable transfected clones. We investigated the effect of transient expression of snail and HRasV12 on luciferase activity in these clones and found that several clones showed altered luciferase activity when transfected with the claudin-4 suppressor (snail, Suppl. Fig. 2A) or the claudin-4 inducer (HRasV12, Suppl. Fig. 2B). TGF-β suppresses claudin-4 expression [23], whereas EGF enhances claudin-4 expression [24]. Therefore, we also investigated the effects of TGF-β and EGF on the luciferase activity in the clones (Suppl. Fig. 2C and D, respectively). Since clone 35 showed the best

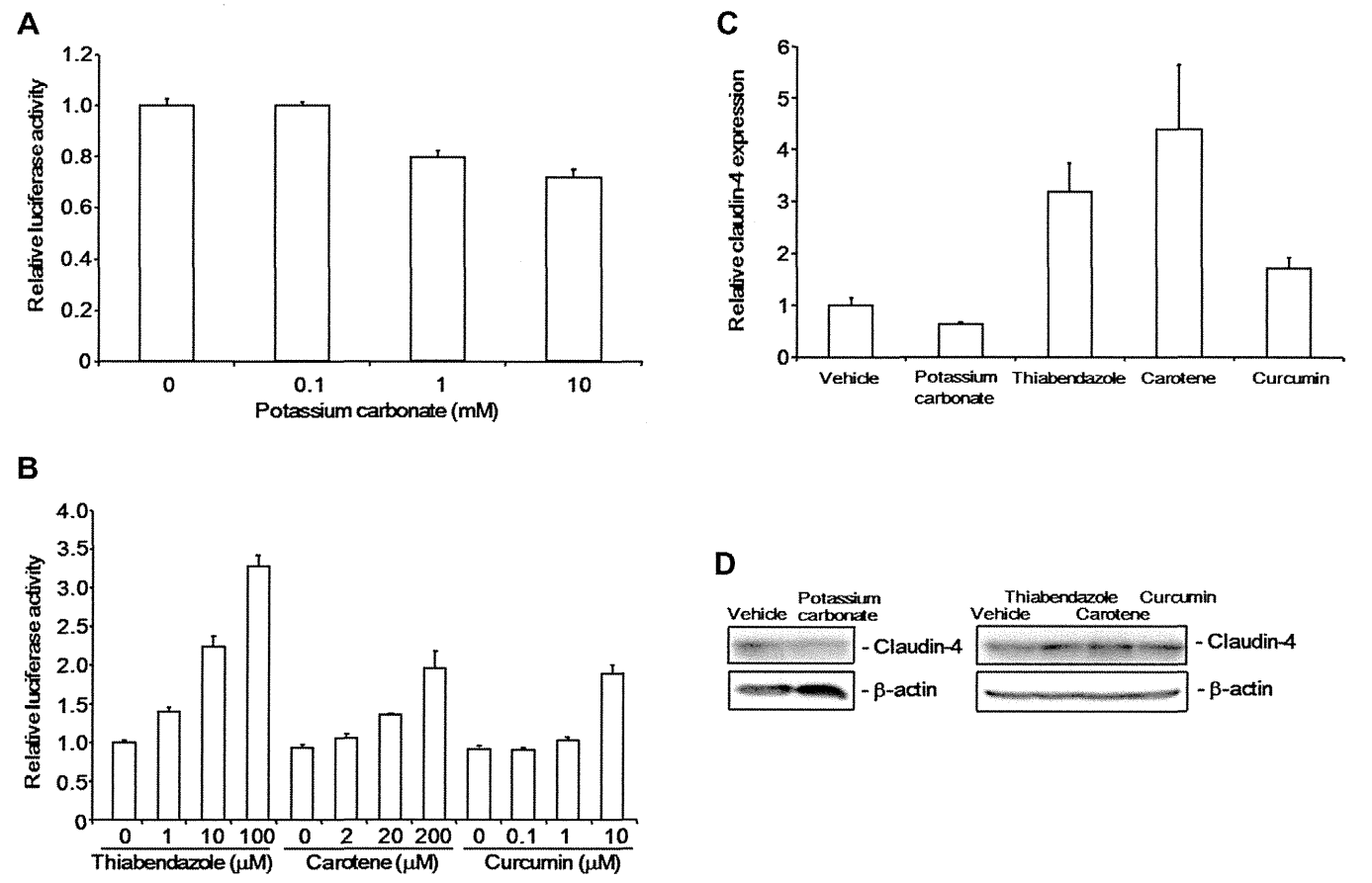

Fig. 3. Screening claudin-4 modulators using the reporter system. (A, B) Dose-dependent effects of the claudin-4 modulator candidates on luciferase expression. Clone 35 cells were treated with potassium carbonate (A), or thiabendazole, carotene, or curcumin (B) at the indicated concentrations for 24 h. Luciferase activity was measured in the lysates. Relative luciferase activity is shown as the ratio of the luciferase activity in the chemical-treated cells to that in the vehicle-treated cells. The data are means ± S.D. ($n = 3$). The results are representative of three independent experiments. (C, D) Effects of the claudin-4 modulator candidates on claudin-4 mRNA expression (C) and claudin-4 protein (D) levels. Clone 35 cells were treated with potassium carbonate (5 mM), thiabendazole (0.1 mM), carotene (0.2 mM), or curcumin (10 μM) for 24 h (C) or 48 h (D). Total RNA was used for qPCR analysis to detect claudin-4 mRNA (C). The relative mRNA expression of claudin-4 normalized to GAPDH expression. The cell lysates were subjected to SDS–PAGE, followed by immunoblotting for claudin-4 (D). GAPDH or β-actin served as loading controls. The result is representative of three independent experiments.

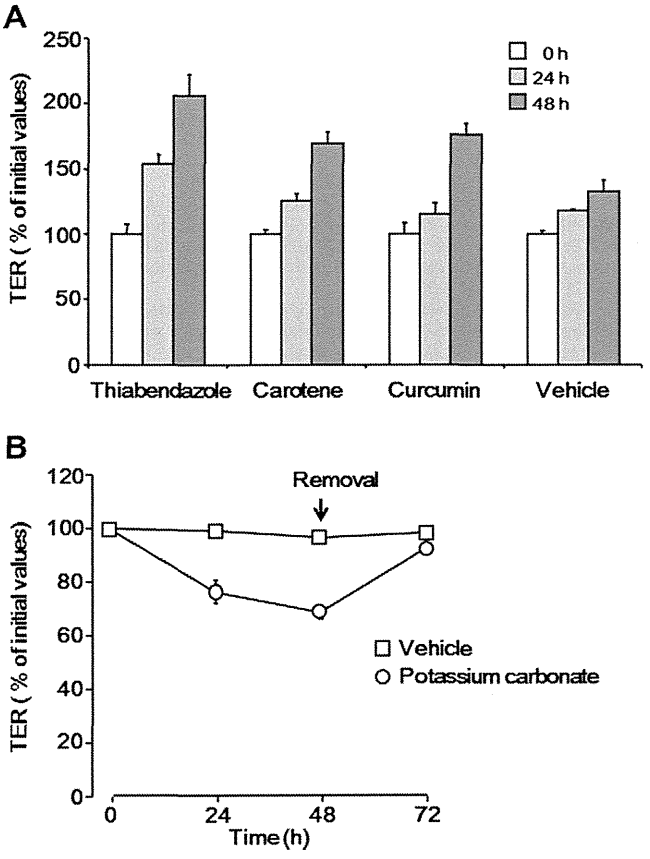

Fig. 4. Effects of claudin-4 modulator on the TJ-barrier in Caco-2 cells. (A) Effect of claudin-4 inducers on the TJ-barrier. Cells were seeded in Transwell™ chambers. Seven days after seeding, the cells were treated with thiabendazole (0.05 mM), carotene (0.2 mM), or curcumin (10 μM). TER values were monitored every 24 h. (B) Effect of a claudin-4 repressor on the TJ-barrier. Cells were seeded in Transwell™ chambers. When the TER values reached a plateau, the TJ-developed cells were treated with potassium carbonate (10 mM). After 48 h of treatment, the medium was replaced with fresh medium. The cells were then cultured for an additional 24 h. TER values were monitored every 24 h. TER values are shown as percentages of the TER values before treatment relative to those in treated cells, as described in the Section 2. The data are means ± S.D. ($n = 3$). These results are representative of three independent experiments.

response to the various claudin-4-modulating treatments, we selected it for further analysis. The clone 35 cells were treated with PMA, which enhances claudin-4 expression [25]. PMA increased luciferase activity in a dose-dependent manner (Fig. 2). These results indicate that clone 35 could be used to screen for modulators of claudin-4 expression.

3.3. Screening for claudin-4 modulators

When we eat, fragments of partially digested food, which still have antigenicity, exist in the intestine. This suggests that claudin modulators that tighten TJ-barriers may be contained in food. Therefore, we screened 86 chemicals used as food additives for claudin-4 modulators (Table 1). At first, we checked the cytotoxicity of these compounds in the clone 35 cells (Table 1). Then, we treated the cells with the compounds at non-toxic concentrations and identified the following claudin-4 modulator candidates: potassium carbonate (No. 3), thiabendazole (No. 68), carotene (No. 83), and curcumin (No. 86) (Suppl. Fig. 3). Each chemical modulated luciferase activity in a dose-dependent manner (Fig. 3A and B). qPCR analysis revealed that thiabendazole, carotene, and curcumin increased claudin-4 expression in the clone 35 cells (Fig. 3C), whereas potassium carbonate decreased claudin-4 expression. Similar results were obtained from Western blot analysis of claudin-4 (Fig. 3D).

To test whether the screened compounds also modulated the TJ-barrier, we investigated the effect of the compounds on the TER value, a marker of TJ-integrity, in Caco-2 cell monolayers, which is a popular model for mucosal barrier. Treatment of cells with thiabendazole, carotene, and curcumin increased the TER values (Fig. 4A). In contrast, potassium carbonate decreased the TER value. Moreover, the TER values recovered when the potassium carbonate was removed (Fig. 4B), and treatment with potassium carbonate did not cause cytotoxicity (data not shown). Thus, we successfully identified claudin-4 modulators.

4. Discussion

Claudin-4 inducers have been the focus of attention in drug development to treat inflammatory diseases and cancers [17–19]; however, their development has been slow. Some chemicals that modulate TJ integrity have been identified: glutamine, bryostatin-1, berberine, quercetin, and butyrate [26–30]. Here, we established a simple monitoring system for claudin-4 expression using a reporter gene, luciferase, and successfully identified chemical claudin-4 modulators: one suppressor of claudin-4 expression, potassium carbonate, and three inducers of claudin-4, thiabendazole, carotene, and curcumin.

Curcumin is an active ingredient of the spice turmeric, which is used in curry powders and as a food preservative. It is also used in traditional medicine to treat various inflammatory conditions, such as arthritis, colitis, and hepatitis [31]. Curcumin has various biological activities, such as anti-inflammatory, anti-oxidant, and anti-cancer effects [32]; however, the underlying mechanisms have never been fully understood. Here, we found that curcumin induces claudin-4 expression and increases TJ integrity. This enhancement of TJ integrity by curcumin may be associated with its therapeutic activities.

Carotene is a precursor of vitamin A. Retinoic acid, a metabolite of vitamin A, enhances TJ integrity in epithelial cells accompanied by expression of claudin-1, -4, and occludin [33]. These findings suggest that metabolized β-carotene-activated expression of claudins enhances the epithelial barrier in Caco-2 cells. Retinoic acid is a biologically active regulator of cell differentiation, proliferation, and apoptosis in various cell types [34]. The activities of retinoic acid are mediated by two types of nuclear receptors: retinoic acid receptors and their heterodimeric counterparts, retinoid X receptors [35]. Specific heterodimer-mediated transcriptional activation increases TJ integrity [36]. The increase in claudin-4 expression and TJ integrity induced by carotene may be caused by the formation of the heterodimer, followed by transcriptional activation.

Thiabendazole is used as a broad spectrum anthelmintic in various animal species and is also used to control parasitic infections in humans [37]. It is also used as an anti-fungal agent for the treatment of fruits [38]. Here, we found that thiabendazole increases claudin-4 expression and TJ integrity, but the mechanism for these activities remains unclear.

Our screening system identified a repressor of intestinal epithelial barrier function as well as three enhancers. We showed that potassium carbonate reduces claudin-4 expression and epithelial barrier function in Caco-2 cells without causing cytotoxicity. Potassium carbonate is used as an acidity regulator, and paracellular permeability is sensitive to pH [39]. Thus, potassium carbonate might reduce epithelial barrier integrity by changing the pH.

In conclusion, we developed the simple screening system for claudin-4 modulator, and we identified several claudin-4 modulators, including three inducers and one repressor. The screening system will thus be a tool for the development of claudin-4

modulators, thereby contributing to basic and pharmaceutical researches.

Acknowledgments

This work was supported by a Grant-in-Aid for Scientific Research from the Ministry of Education, Culture, Sports, Science, and Technology, Japan (21689006; 24390042), by a Health and Labor Sciences Research Grant from the Ministry of Health, Labor, and Welfare of Japan and by the Takeda Science Foundation.

Appendix A. Supplementary data

Supplementary data associated with this article can be found, in the online version, at http://dx.doi.org/10.1016/j.bbrc.2012.08.083.

References

[1] M. Cereijido, R.G. Contreras, L. Shoshani, D. Flores-Benitez, I. Larre, Tight junction and polarity interaction in the transporting epithelial phenotype, Biochim. Biophys. Acta 1778 (2008) 770–793.
[2] D.W. Powell, Barrier function of epithelia, Am. J. Physiol. 241 (1981) G275–288.
[3] A. Wodarz, I. Nathke, Cell polarity in development and cancer, Nat. Cell Biol. 9 (2007) 1016–1024.
[4] B.J. Aungst, Intestinal permeation enhancers, J. Pharm. Sci. 89 (2000) 429–442.
[5] M. Kondoh, T. Yoshida, H. Kakutani, K. Yagi, Targeting tight junction proteins-significance for drug development, Drug Discovery Today 13 (2008) 180–186.
[6] H. Chiba, M. Osanai, M. Murata, T. Kojima, N. Sawada, Transmembrane proteins of tight junctions, Biochim. Biophys. Acta 1778 (2008) 588–600.
[7] L.L. Mitic, V.M. Unger, J.M. Anderson, Expression, solubilization, and biochemical characterization of the tight junction transmembrane protein claudin-4, Protein Sci. 12 (2003) 218–227.
[8] M. Furuse, S. Tsukita, Claudins in occluding junctions of humans and flies, Trends Cell Biol. 16 (2006) 181–188.
[9] K. Morita, M. Furuse, K. Fujimoto, S. Tsukita, Claudin multigene family encoding four-transmembrane domain protein components of tight junction strands, Proc. Natl. Acad. Sci. USA 96 (1999) 511–516.
[10] M. Furuse, M. Hata, K. Furuse, Y. Yoshida, A. Haratake, Y. Sugitani, T. Noda, A. Kubo, S. Tsukita, Claudin-based tight junctions are crucial for the mammalian epidermal barrier: a lesson from claudin-1-deficient mice, J. Cell Biol. 156 (2002) 1099–1111.
[11] A. Gow, C.M. Southwood, J.S. Li, M. Pariali, G.P. Riordan, S.E. Brodie, J. Danias, J.M. Bronstein, B. Kachar, R.A. Lazzarini, CNS myelin and sertoli cell tight junction strands are absent in Osp/claudin-11 null mice, Cell 99 (1999) 649–659.
[12] T. Nitta, M. Hata, S. Gotoh, Y. Seo, H. Sasaki, N. Hashimoto, M. Furuse, S. Tsukita, Size-selective loosening of the blood–brain barrier in claudin-5-deficient mice, J. Cell Biol. 161 (2003) 653–660.
[13] P.J. Morin, Claudin proteins in human cancer: promising new targets for diagnosis and therapy, Cancer Res. 65 (2005) 9603–9606.
[14] J.D. Schulzke, S. Ploeger, M. Amasheh, A. Fromm, S. Zeissig, H. Troeger, J. Richter, C. Bojarski, M. Schumann, M. Fromm, Epithelial tight junctions in intestinal inflammation, Ann. N. Y. Acad. Sci. 1165 (2009) 294–300.
[15] N. Sonoda, M. Furuse, H. Sasaki, S. Yonemura, J. Katahira, Y. Horiguchi, S. Tsukita, *Clostridium perfringens* enterotoxin fragment removes specific claudins from tight junction strands: evidence for direct involvement of claudins in tight junction barrier, J. Cell Biol. 147 (1999) 195–204.
[16] H. Uchida, M. Kondoh, T. Hanada, A. Takahashi, T. Hamakubo, K. Yagi, A claudin-4 modulator enhances the mucosal absorption of a biologically active peptide, Biochem. Pharmacol. 79 (2010) 1437–1444.
[17] R. Mennigen, K. Nolte, E. Rijcken, M. Utech, B. Loeffler, N. Senninger, M. Bruewer, Probiotic mixture VSL#3 protects the epithelial barrier by maintaining tight junction protein expression and preventing apoptosis in a murine model of colitis, Am. J. Physiol. 296 (2009) G1140–1149.
[18] S.K. Lee, J. Moon, S.W. Park, S.Y. Song, J.B. Chung, J.K. Kang, Loss of the tight junction protein claudin 4 correlates with histological growth-pattern and differentiation in advanced gastric adenocarcinoma, Oncol. Rep. 13 (2005) 193–199.
[19] S. Mima, S. Tsutsumi, H. Ushijima, M. Takeda, I. Fukuda, K. Yokomizo, K. Suzuki, K. Sano, T. Nakanishi, W. Tomisato, T. Tsuchiya, T. Mizushima, Induction of claudin-4 by nonsteroidal anti-inflammatory drugs and its contribution to their chemopreventive effect, Cancer Res. 65 (2005) 1868–1876.
[20] H. Honda, M.J. Pazin, H. Ji, R.P. Wernyj, P.J. Morin, Crucial roles of Sp1 and epigenetic modifications in the regulation of the CLDN4 promoter in ovarian cancer cells, J. Biol. Chem. 281 (2006) 21433–21444.
[21] T. Vincent, E.P. Neve, J.R. Johnson, A. Kukalev, F. Rojo, J. Albanell, K. Pietras, I. Virtanen, L. Philipson, P.L. Leopold, R.G. Crystal, A.G. de Herreros, A. Moustakas, R.F. Pettersson, J. Fuxe, A SNAIL1-SMAD3/4 transcriptional repressor complex promotes TGF-beta mediated epithelial–mesenchymal transition, Nat. Cell Biol. 11 (2009) 943–950.
[22] J. Ikenouchi, M. Matsuda, M. Furuse, S. Tsukita, Regulation of tight junctions during the epithelium–mesenchyme transition: direct repression of the gene expression of claudins/occludin by snail, J. Cell Sci. 116 (2003) 1959–1967.
[23] P. Michl, C. Barth, M. Buchholz, M.M. Lerch, M. Rolke, K.H. Holzmann, A. Menke, H. Fensterer, K. Giehl, M. Lohr, G. Leder, T. Iwamura, G. Adler, T.M. Gress, Claudin-4 expression decreases invasiveness and metastatic potential of pancreatic cancer, Cancer Res. 63 (2003) 6265–6271.
[24] A. Ikari, K. Atomi, A. Takiguchi, Y. Yamazaki, M. Miwa, J. Sugatani, Epidermal growth factor increases claudin-4 expression mediated by Sp1 elevation in MDCK cells, Biochem. Biophys. Res. Commun. 384 (2009) 306–310.
[25] C. Wray, Y. Mao, J. Pan, A. Chandrasena, F. Piasta, J.A. Frank, Claudin-4 augments alveolar epithelial barrier function and is induced in acute lung injury, Am. J. Physiol. 297 (2009) L219–227.
[26] L. Gu, N. Li, Q. Li, Q. Zhang, C. Wang, W. Zhu, J. Li, The effect of berberine in vitro on tight junctions in human Caco-2 intestinal epithelial cells, Fitoterapia 80 (2009) 241–248.
[27] N. Li, V.G. DeMarco, C.M. West, J. Neu, Glutamine supports recovery from loss of transepithelial resistance and increase of permeability induced by media change in Caco-2 cells, J. Nutr. Biochem. 14 (2003) 401–408.
[28] L. Peng, Z.R. Li, R.S. Green, I.R. Holzman, J. Lin, Butyrate enhances the intestinal barrier by facilitating tight junction assembly via activation of AMP-activated protein kinase in Caco-2 cell monolayers, J. Nutr. 139 (2009) 1619–1625.
[29] T. Suzuki, H. Hara, Quercetin enhances intestinal barrier function through the assembly of zonula [corrected] occludens-2, occludin, and claudin-1 and the expression of claudin-4 in Caco-2 cells, J. Nutr. 139 (2009) 965–974.
[30] J. Yoo, A. Nichols, J.C. Song, J. Mammen, I. Calvo, R.T. Worrell, J. Cuppoletti, K. Matlin, J.B. Matthews, Bryostatin-1 attenuates TNF-induced epithelial barrier dysfunction: role of novel PKC isozymes, Am. J. Physiol. 284 (2003) G703–712.
[31] J. Epstein, I.R. Sanderson, T.T. Macdonald, Curcumin as a therapeutic agent: the evidence from in vitro, animal and human studies, Br. J. Nutr. 103 (2010) 1545–1557.
[32] R.K. Maheshwari, A.K. Singh, J. Gaddipati, R.C. Srimal, Multiple biological activities of curcumin: a short review, Life Sci. 78 (2006) 2081–2087.
[33] M. Osanai, N. Nishikiori, M. Murata, H. Chiba, T. Kojima, N. Sawada, Cellular retinoic acid bioavailability determines epithelial integrity: role of retinoic acid receptor alpha agonists in colitis, Mol. Pharmacol. 71 (2007) 250–258.
[34] M. Osanai, M. Petkovich, Expression of the retinoic acid-metabolizing enzyme CYP26A1 limits programmed cell death, Mol. Pharmacol. 67 (2005) 1808–1817.
[35] P. Kastner, M. Mark, P. Chambon, Nonsteroid nuclear receptors: what are genetic studies telling us about their role in real life?, Cell 83 (1995) 859–869
[36] H. Kubota, H. Chiba, Y. Takakuwa, M. Osanai, H. Tobioka, G. Kohama, M. Mori, N. Sawada, Retinoid X receptor alpha and retinoic acid receptor gamma mediate expression of genes encoding tight-junction proteins and barrier function in F9 cells during visceral endodermal differentiation, Exp. Cell Res. 263 (2001) 163–172.
[37] K. Walton, R. Walker, J.J. van de Sandt, J.V. Castell, A.G. Knapp, G. Kozianowski, M. Roberfroid, B. Schilter, The application of in vitro data in the derivation of the acceptable daily intake of food additives, Food Chem. Toxicol. 37 (1999) 1175–1197.
[38] J.P. Groten, W. Butler, V.J. Feron, G. Kozianowski, A.G. Renwick, R. Walker, An analysis of the possibility for health implications of joint actions and interactions between food additives, Regul. Toxicol. Pharmacol. 31 (2000) 77–91.
[39] V.W. Tang, D.A. Goodenough, Paracellular ion channel at the tight junction, Biophys. J. 84 (2003) 1660–1673.

Biochemical and Biophysical Research Communications 423 (2012) 229–233

Contents lists available at SciVerse ScienceDirect

Biochemical and Biophysical Research Communications

journal homepage: www.elsevier.com/locate/ybbrc

Comparison of mucosal absorption-enhancing activity between a claudin-3/-4 binder and a broadly specific claudin binder

Koji Matsuhisa, Masuo Kondoh *, Hidehiko Suzuki, Kiyohito Yagi

Laboratory of Bio-Functional Molecular Chemistry, Graduate School of Pharmaceutical Sciences, Osaka University, Osaka, Japan

ARTICLE INFO

Article history:
Received 11 May 2012
Available online 31 May 2012

Keywords:
Tight junction
Claudin
Clostridium perfringens enterotoxin
Mucosal absorption

ABSTRACT

Intercellular spaces between adjacent mucosal epithelial cells are sealed by tight junctions (TJs) that prevent the free movement of solutes across the epithelium. Claudins (CLs), a family of 27 integral membrane proteins, are essential components for TJ seals. We previously used a CL-3/-4 binder, the C-terminal fragment of *Clostridium perfringens* enterotoxin (C-CPE), to show that CL modulation is a promising method to enhance mucosal absorption. Recently, by using a C-CPE mutant library, we developed a CL binder (m19) with broad specificity to CL-1, -2, -4, and -5. Here, we compared the mucosal absorption-enhancing activity of C-CPE and m19. Both CL binders enhanced jejunal absorption of dextran with a molecular mass of 4000 and 150,000 Da and nasal absorption of dextran with a mass of 4000 Da but not 150,000 Da in rats. Although both binders showed similar nasal absorption-enhancing activity of dextran (4000 Da), m19 exhibited a more potent jejunal absorption-enhancing effect than that of C-CPE. These findings suggest that mucosal absorption-enhancing activity may be modified by modulating CL specificity.

1. Introduction

Recent drug discovery has shifted to the development of biologics, including nucleic acids, peptides, and proteins; these biologics represent over 30% of the new drugs worldwide. Most biologics are injected into patients because of their poor permeability that stems from their hydrophilic and degradable properties. Non-invasive drug delivery to the systemic circulation remains an important challenge.

Epithelium surrounds organisms and separates interior and outer bodies. Passage through epithelium is the first step in drug absorption. Routes for solute movement across epithelium are classified into transcellular and paracellular routes. Since the 1990s, various methods have been developed to deliver drugs via the transcellular route, including the use of simple diffusion and transporter- and receptor-mediated active transport. Some of these methods have been used for chemicals; however, the transcellular approaches have mainly been used for biologics [1,2]. Disrupting the intercellular seal has been the basic strategy for drug delivery via the paracellular route. Paracellular drug delivery has been studied for over 40 years, but its application to clinical use remains limited because of damage to the mucosal membrane [3,4].

Tight junctions (TJs), localized between adjacent epithelial cells, seal the intercellular space to prevent leakage of solutes across the epithelial cell sheets. Modulation of TJ-barriers has been a popular method to enhance epithelial absorption of drugs. However, the biochemical and functional structures of TJs had not been identified before 1998. Freeze-fracture replica electron microscopy analysis had shown that TJs form a series of continuous, anastomotic, and intramembranous particle strands [5], but in 1998, the first structural and functional component of TJs, claudin (CL), was identified [6]. CL is a tetra-transmembrane protein with a molecular mass of ~23 kDa; the CL family comprises 27 members [7,8]. Interestingly, the expression profiles and barrier-functions of the various CL family members differ among tissues. For instance, CL-1-deficient mice exhibit loss of the epidermal barrier, and CL-5-deficient mice show disruption of the blood–brain barrier [9,10]. The CLs are believed to form homo- and hetero-type strands on the lateral membrane of TJs [7,11], and the combination of CLs is thought to determine the properties of the TJ seals. Extensive research on CLs has provided insights into strategies for drug delivery via the paracellular route that involve modulating CLs.

Clostridium perfringens enterotoxin (CPE), a 35-kDa polypeptide, is a food poison in humans [12]. CPE binds via its C-terminal

Abbreviations: TJ, tight junction; CL, claudin; C-CPE, C-terminal fragment of *Clostridium perfringens* enterotoxin from 194 to 319 amino acids; CPE, *Clostridium perfringens* enterotoxin; FD-4, fluorescent labeled dextran with a molecular mass of 4000 Da; FD-150, fluorescent labeled dextran with a molecular mass of 150,000 Da; FBS, fetal bovine serum; BSA, bovine serum albumin; AUC, the area under the plasma concentration curve.

* Corresponding author. Address: Laboratory of Bio-Functional Molecular Chemistry, Graduate School of Pharmaceutical Sciences, Osaka University, Suita, Osaka 565-0871, Japan. Fax: +81 6 6879 8199.

E-mail address: masuo@phs.osaka-u.ac.jp (M. Kondoh).

0006-291X/$ - see front matter © 2012 Elsevier Inc. All rights reserved.
http://dx.doi.org/10.1016/j.bbrc.2012.05.060

region, and a receptor of CPE is identical to CL-3/-4 [13–15]. Interestingly, the C-terminal receptor binding fragment of CPE reversibly modulates TJ barriers *in vitro*. We previously found that the C-terminal fragment of CPE, which corresponds to amino acids 184–319, is 400-fold more potent than the clinically used absorption enhancer sodium caprate in terms of its jejunal absorption-enhancing effect of dextran (4000 Da) and that this absorption-enhancing activity involves an interaction between the CPE fragment and CL-4 [16]. We also showed that a CL binder corresponding to amino acids 194–319 of CPE, called here C-CPE, enhances jejunal, pulmonary, and nasal absorption of a biologically active peptide [17]. Thus, we have established proof-of-concept for CL-targeted mucosal absorption of drugs by using CPE fragments. We also examined the functional domain map of C-CPE by using site-directed mutagenesis [18,19], and developed a C-CPE library containing randomly mutated functional residues, which we used as a CL binder screening system with a baculoviral display [20]. By using this system, we identified the broadly specific claudin binder m19 from the C-CPE mutant library [21]. Here, we compared the mucosal absorption-enhancing activity of C-CPE with that of the broadly specific claudin binder m19.

2. Materials and methods

2.1. Materials

Fluorescent-labeled dextrans with molecular masses of 4000 Da (FD-4) or 150,000 Da (FD-150) were purchased from Sigma–Aldrich (St. Louis, MO). A mouse fibroblast cell line (L cells) and mouse CL-1-, CL-2-, CL-4-, or CL-5-expressing L cells (CL-1/L cells, CL-2/L cells, CL-4/L cells, CL-5/L cells) were kindly provided by Dr. S. Tsukita (Kyoto University, Kyoto, Japan). Anti-His-tag antibody was obtained from Thermo Fisher Scientific Inc. (Waltham, MA). All reagents used were of research grade.

2.2. Fluorescence-activated cell sorting

The CL/L cells were maintained in modified Eagle's medium supplemented with 10% fetal bovine serum (FBS) in a 5% CO_2 atmosphere at 37 °C. The cells were resuspended in the culture medium. Cells (5.0×10^5 cells) were incubated with C-CPEs for 1 h at 4 °C. The cells were then washed with phosphate buffered saline (PBS) containing 0.1% bovine serum albumin (BSA) twice, and then incubated with an anti C-CPE-fused tag (histidine) antibody. The cells were incubated with fluorescein-labeled secondary antibody, and C-CPE-bound cells were detected and analyzed with a flow cytometer and appropriate software (FACSCalibur and CellQuest, Becton Dickinson, New Jersey, USA).

2.3. Preparation of C-CPE

C-CPE and the broadly specific CL binder m19 were prepared as described previously [17,21]. Briefly, pET16b plasmids encoding C-CPE or m19 were transduced into *Escherichia coli* strain BL21 (DE3), and production of the recombinant proteins was induced by the addition of isopropyl-D-thiogalactopyranoside. The harvested cells were lysed in buffer A (10 mM Tris–HCl, pH 8.0, 400 mM NaCl, 5 mM $MgCl_2$, 0.1 mM phenylmethanesulfonyl fluoride, 1 mM 2-mercaptoethanol, and 10% glycerol). The lysates were applied to a HiTrap™ Chelating HP column (GE Healthcare, Buckinghamshire, UK), and the recombinant proteins were eluted with buffer A containing imidazole. The buffer was exchanged with PBS by using a PD-10 column (GE Healthcare), and the purified protein was stored at −80 °C until use. Purification of the recombinant proteins was confirmed by means of sodium dodecyl sulfate–polyacrylamide gel electrophoresis (SDS–PAGE), followed by staining with Coomassie Brilliant Blue. Protein was quantified with a BCA protein assay kit in which BSA served as the standard (Pierce Chemical, Rockford, IL).

2.4. In situ loop assay

Jejunal absorption of FD-4 or FD-150 was evaluated by using an *in situ* loop assay as described previously [16]. The experiments were performed according to the guidelines of the ethics committee of Osaka University. After 7-week-old Wister male rats were anesthetized with thiamylal sodium, a midline abdominal incision was made, and the jejunum was washed with PBS. A 5-cm long jejunal loop was prepared by closing both ends with sutures. A mixture of FDs (2 mg) and CL binder (200 μg) was injected into the jejunal loop. Blood was collected from the jugular vein at the indicated time points. The plasma levels of FDs were measured with a fluorescence spectrophotometer (Tristar LBP941; Berthold Technologies, Bad Wildbad, Germany). The area under the plasma concentration curve (AUC) of the FDs from 0 to 4 h was calculated by using the trapezoidal method.

2.5. Nasal absorption assay

Nasal absorption of FDs was examined in 7-week-old Wister male rats. The experiments were performed according to the guidelines of the ethics committee of Osaka University. For the nasal absorption assay, a mixture of FDs (2 mg) and CL binder (50 μg) was intranasally injected into both sides of the nasal cavity. The total injection volume did not exceed 50 μl. Blood was collected at the indicated time points, and the plasma concentration of the FDs was measured with a fluorescence spectrophotometer, as described above.

2.6. Statistical analysis

Data were analyzed by using Dunnett's multiple comparison test; statistical significance was assigned at $p < 0.05$.

3. Results

Previously, we found that m19 binds to CL-1, -2, -4, and -5-expressing cells [21]. However, because approximately half of the CL molecule is embedded in the cell membrane, it is very hard to prepare recombinant CL proteins. Therefore, we first compared the affinities of C-CPE and m19 for CLs by using a flow cytometer and found that C-CPE bound to CL-4 whereas m19 bound to CL-1, -2, -4, and -5 (Fig. 1).

To investigate jejunal absorption of FD-4 and FD-150, we performed an *in situ* loop assay. C-CPE and m19 enhanced jejunal absorption of FD-4 (AUC from 0 to 4 h = 18.33 ± 3.12 μg h/ml and 31.91 ± 2.03 μg h/ml, respectively, Fig. 2A and B). C-CPE and m19 were more potent enhancers of jejunal absorption of FD-4 than of FD-150. Although C-CPE did not enhance jejunal absorption of FD-150, m19 did increase jejunal absorption of the larger dextran (Fig. 2C and D). C-CPE and m19 also increased nasal absorption of FD-4 (Fig. 3A and B); however, the absorption-enhancing effects were much weaker than those in the jejunum (AUC from 0 to 4 h: 1.52 ± 0.23 μg h/ml and 1.73 ± 0.16 μg h/ml, respectively). Neither C-CPE nor m19 enhanced nasal absorption of FD-150 (Fig. 3C and D). Thus, the absorption-enhancing activities of C-CPE and m19 differ.

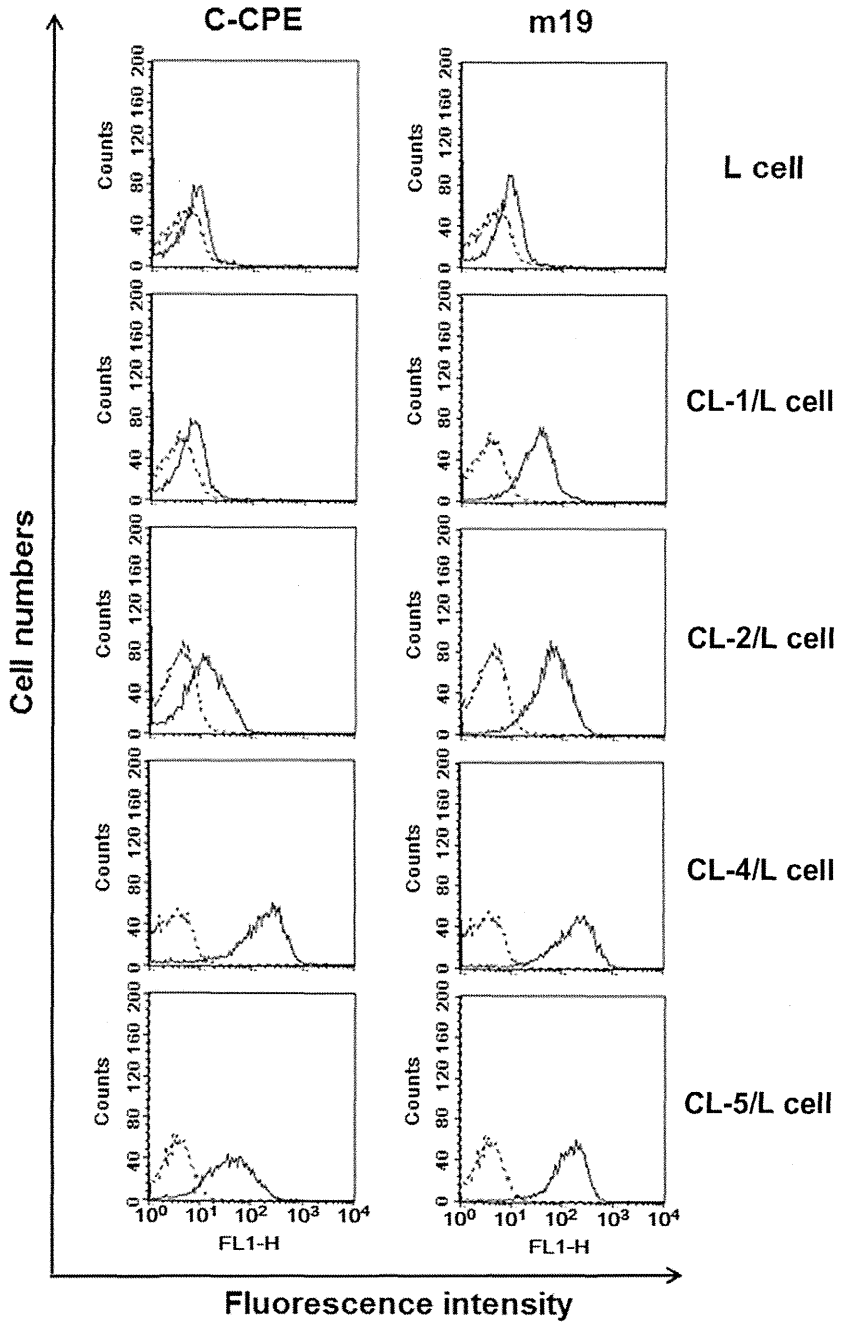

Fig. 1. Fluorescence-activated cell sorting analysis of the affinity of C-CPE and m19 for claudins. Cells were incubated with 10 μg/ml of C-CPE or m19 for 1 h at 4 °C. They were then washed twice with PBS before being incubated with a mouse anti-His-tag antibody. The cells were then incubated with fluorescent-labeled anti-mouse IgG. The cells were subjected to FACS analysis as described in the Section 2. The dotted histograms show cells treated with the anti-His-tag antibody and fluorescent-labeled IgG. The solid histograms show cells treated with C-CPE or m19, the anti-His-tag antibody, and fluorescent-labeled IgG.

4. Discussion

TJs contain several CLs, and the combination and mixing ratios of CL family members determine the barrier properties of the TJ seals [11,22]. Accordingly, a change in CL specificity may lead to a change in the absorption-enhancing properties of CL binders. Here, we compared the mucosal absorption-enhancing effects of a CL-3/-4 binder, C-CPE, with those of a CL-1/-2/-4/-5 binder, m19, and found that m19, the binder with the broader specificity, was a more potent jejunal absorption enhancer, but had similar nasal absorption-enhancing activity compared with C-CPE.

Heterogeneity of CL expression has been observed among tissues [23], including the gut, where heterogeneic CL subcellular localization has also been observed [7,24]. CL-8 is expressed in the ileum and colon, but not in the duodenum and jejunum. CL-4 expression is lower in the jejunum than in the colon. The C-terminal fragment of CPE, which corresponds to amino acids 184–319, enhances jejunal not colonic absorption of FD-4 [16]. Segment-specific expression of CLs has also been observed in kidney [7]. One possible explanation for the different mucosal absorption-enhancing effects of C-CPE and m19 in jejunal and nasal mucosa may be found in the tissue-specific heterogeneity of CL expression. CLs form homo- and hetero-type strands in TJs and the CL combination determines the properties of the TJ barriers [11,22]. CL-11 expression decreases TJ integrity in LLC-PK1 cells, but increases it in MDCK-II cells [25]. CL-4 expression, however, increases TJ integrity